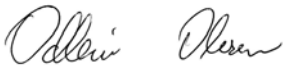


GEOLOGI FOR SAMFUNNET

GEOLOGY FOR SOCIETY



Report no.: 2008.012		ISSN 0800-3416	Grading: Confidential until 31.12.2009
Title: Lithospheric structure and tectonic setting of the greater Barents Sea Region			
Authors: Jörg Ebbing, Carla Braitenberg, Susanne Buitter, Susann Wienecke, Cécile Barrère, Laura Marelllo and Jan Reidar Skilbrei		Client: StatoilHydro	
County:		Commune:	
Map-sheet name (M=1:250.000)		Map-sheet no. and -name (M=1:50.000)	
Deposit name and grid-reference:		Number of pages: 51	Price (NOK):
		Map enclosures:	
Fieldwork carried out:	Date of report: 31.01.2008	Project no.: 3133.00	Person responsible: 
<p>Summary:</p> <p>The Barents Sea is characterised by deep basins in the western and eastern Barents Sea, and large-scale differences in the lithospheric structure, which reflect the different tectonic history and basin forming processes. The western Barents Sea is associated with typical rift basins, while the eastern Barents Sea features large-scale megabasins, which are not typical rift basins. Isostatic as well as seismological studies point towards a heterogeneous upper mantle with high-density material underlying the megabasins. A global study of large-scale basins shows that isostatic balance is often achieved by densification of the lower crust or upper mantle. These structures are expressed in geoid anomalies, but are associated with small density contrasts, which make detailed imaging difficult. However, the high-density structures in the upper mantle appear to have a generic link to the basin formation.</p> <p>The magnetic anomalies in the Barents Sea point towards the presence of an intra-crustal intrusive along the transition zone between the rift basin setting to the megabasin setting, which is also visible in the gravity signal and isostatic results. While the eastern Barents Sea appears to be under Timanian influence, the western Barents Sea is clearly influenced by Caledonian tectonic events and the Mesozoic break-up of the North Atlantic region, as also evident from detailed basement models based on seismic and potential field interpretation. Studies of regional isostasy are as yet not conclusive, but show the importance of the intra-crustal density distribution in models at the lithospheric and basin scale.</p>			
Keywords: Gravimetry		Magnetometry	Report
Continental Shelf		Isostasy	Geophysics
Research			

CONTENTS

1 Introduction	4
2 Background data of the Barents Sea Region.....	6
2.1 Basement depth models	7
2.2 Barents50, BARMOD and Barents 3D.....	8
2.3 Gravity and magnetic data.....	10
3 Forward gravity modelling and the isostatic state of the Barents Sea Region.....	13
3.4 Isostatic state of the Barents Sea Region.....	15
3.5 Lithospheric isostasy - results.....	17
3.6 Comparison of mantle structure to basin outline, the geoid and upper mantle velocities.....	21
4 Basement characterization and basin characteristics	27
4.7 Comparison of crustal structure to basin outline and magnetic field data.....	27
4.8 Western Barents Sea.....	29
4.9 Eastern Barents Sea	30
5 Rheological modelling to identify connections between flexural rigidity and crustal structures	33
5.10 Inverse flexural modelling with ASEP	34
5.11 Forward numerical modelling	35
5.12 Discussion of elastic thickness estimates	37
6 Discussion and outlook	40
Acknowledgements	43
References	44
Lits of Figures	49

1 INTRODUCTION

This report summarizes the results of the project “Lithospheric structure and tectonic setting of the greater Barents Sea Region”, which was carried out at the Geological Survey of Norway in cooperation with the University of Trieste and with financial support from Statoil ASA (now StatoilHydro). The project was initiated in 2005 as a continuation of a project discussing the isostatic state of the Barents Sea (Ebbing et al. 2005) and continued to the end of 2007. Within the project period, the following sub-topics have been studied:

- A. 3D density model of the greater Barents Sea Region (Chapter 3)
- B. Forward and inverse regional isostatic modelling (Chapter 3)
- C. Study of mantle densities and crustal residuals and comparison to the magnetic anomalies (Chapter 3 & 4)
- D. Rheological modelling to identify links between flexural rigidity and crustal structures (Chapter 5)
- E. Tectonic synthesis: identifying deformation fronts and sutures (Chapter 6)
- F. Global intra-cratonic basin studies to further understand the East Barents Sea basins (Chapter 4 & 6)

Details of the individual studies have been presented in a series of NGU reports (Ebbing et al. 2005, Braitenberg & Ebbing 2006, 2007, Wienecke et al. 2007, Buitter 2007) and publications (Ebbing et al. 2007a). The reader is referred to the individual reports for details of the applied methodologies and their mathematical formulation. Here we summarize the main results from the different sub-projects and discuss the implications of the integrated results for the knowledge of the tectonic history of the Barents Sea Region.

In this report, we also use studies performed in the framework of the HeatBar and PETROBAR projects at NGU and results of the seismological project Barents3D at the University of Oslo, which is carried out in cooperation with NORSAR and USGS. Some spin-off activities of our project have been transferred to the PETROBAR project, which started in 2007 and continues into 2010. Within this project new information will be made available, which will hopefully overcome some of the unknowns and uncertainties which became evident in the course of our project.

The original motivation for the project was that despite the large amount of industrial data available in the Norwegian and easternmost Russian Barents Sea, only a few regional studies existed that integrate the eastern and western Barents Sea regions (e.g. Johansen et al. 1992). Thus, many key questions related to the tectonic setting and the structure of the continental shelf area of the Barents Sea Region are not yet answered, even though its hydrocarbon potential is the subject of increased scientific and economic interest. Here, we try to give new insights and new information, which will help to understand the tectonic evolution of the Barents Sea and the mechanisms forming its sedimentary basins.

2 BACKGROUND DATA OF THE BARENTS SEA REGION

Industrial and academic geophysical studies reveal that the Barents Sea basins have a relatively complete succession of sedimentary strata, but their characteristics are different in the western and eastern Barents Sea (e.g. Fichler et al. 1997, Johansen et al. 1992, Gramberg et al. 2001). Basins in the western Barents Sea region have a depth of up to 14 km and are generally narrow compared to the broad basins in the eastern Barents Sea that have a maximum thickness of 20 km (Figs. 2.1 and 2.2). The western Barents Sea basins are generally interpreted to be rift basins (e.g. Faleide et al. 1993, 1996), but there is no universal agreement on the underlying cause of formation of the South and North eastern Barents Sea basins (e.g. Gramberg et al. 2001, Ritzmann et al. 2007, O'Leary et al. 2004).

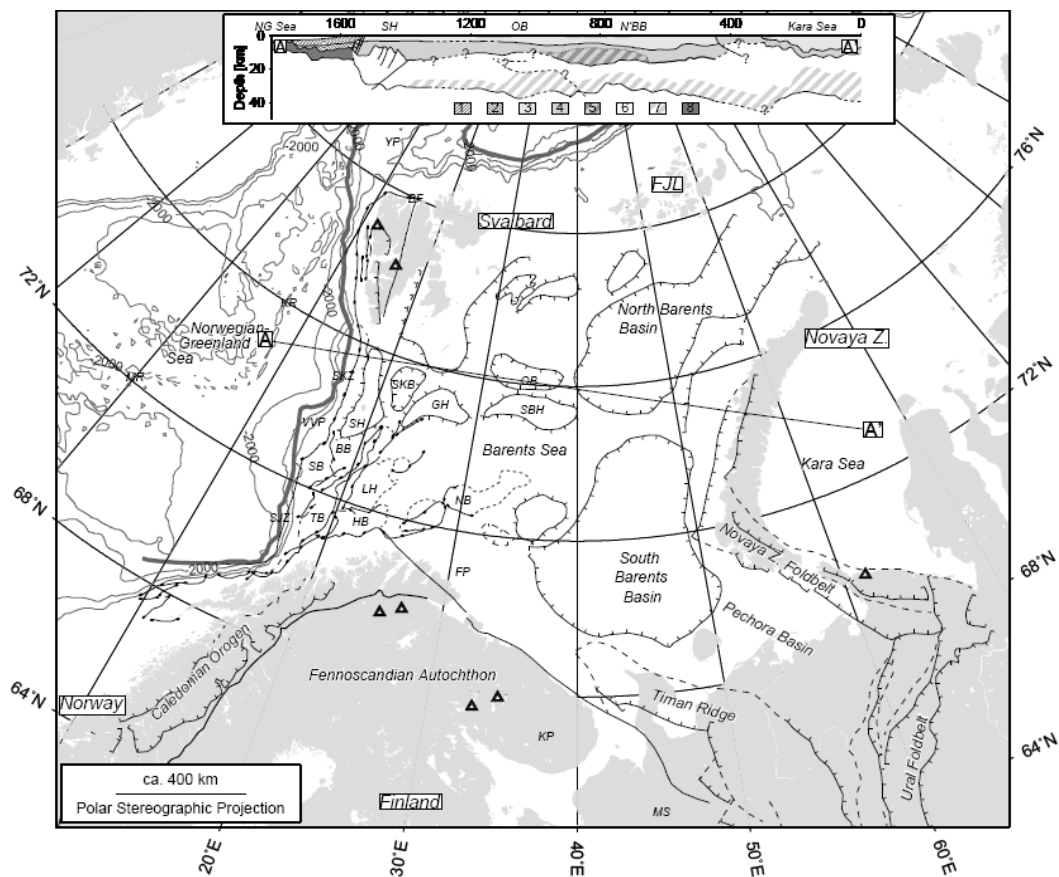


Figure 2.1 Overview map of the Barents Sea and surrounding regions (redrawn from Ritzmann et al. 2007). BB: Bjørnøya Basin; BF: Billefjorden Fault; FP: Finnmark Platform; FJL: Franz-Josef Land; GH: Gardabanken High; HB: Hammerfest Basin; KP: Kola Peninsula; KR: Knipovich Ridge; LH: Loppa High; MR: Mohns Ridge; MS: Mezen Syncline; NB: Nordkapp Basin; OB: Olga Basin; SB: Sørvestnaget Basin; SBH: Sentralbanken High; SH: Stappen High; SKB: Sørkapp Basin; SKZ: Sørkapp Fault Zone; SJZ: Senja Fracture Zone; TB: Tromsø Basin; VVP: Vestbakken Volcanic Province; YP: Yermak Plateau. Top insert shows a geological profile from the Knipovich Ridge to the Kara Sea (A-A').

2.1 Basement depth models

Estimates of the top basement for the Barents Sea are mainly based on aeromagnetic depth-source estimates (e.g. Skilbrei 1991, 1995) combined with shallow and deep seismic lines (e.g. Johansen et al. 1992, Gramberg et al. 2001, Ritzmann et al. 2007). These studies focus on either the western or eastern Barents Sea or have only limited resolution along the transition between the two areas. To date, gravity field interpretation has been used only to a minor extent in compiling top basement maps (e.g. Gramberg et al. 2001).

The compilation presented by Skilbrei (1991, 1995) is based on aeromagnetic depth-source estimates combined with a variety of industrial shallow and deep seismic lines. This leads to a high resolution (5x5 km), but the dataset is only available for the southwestern Barents Sea. In general, the accuracy of the depth to basement estimates from the aeromagnetic data is of the order of +/- 1 km for the deepest part of the basins, but this estimate also depends on the available constraints from seismic data (Skilbrei 1991).

The depth to basement compilation of Gramberg et al. (2001) is based on the interpretation of some thousand kilometres of reflection and refraction lines. Interpretation of aeromagnetic surveys and gravity observations were also used to identify the depth to basement. Even if the study by Gramberg et al. (2001) seems to rely on an extensive database, an unambiguous evaluation of the compilations is not possible, as a detailed description is only available in archive data at VNIIOkeangeologia, St. Petersburg.

The basement map in Fig. 2.2 combines the recent compilation "Barents50" by Ritzmann et al. (2007; see details below) and the compilation by Skilbrei (1991, 1995). The basement compilation is best constrained along the available 2D wide-angle lines. Across the transition zone, a composite seismic interpretation (Bungum et al. 2005) and some industry data are available.

In the eastern Barents Sea, the compilation of Ritzmann et al. (2007) is in general agreement with studies by Johansen et al. (1992) and Gramberg et al. (2001). While the overall basement shape is similar in these studies, the biggest difference is evident in the area of maximum depth to basement in the central eastern Barents Sea. The compilation by Gramberg et al. (2001) features a deep basement in the southeast Barents Sea, while the compilation of Johansen et al. (1992) shows the deepest basement in the northeast Barents Sea and less

prominent occurrence of sediments in the southeast Barents Sea. Differences in the basement depths can be explained by varying geophysical interpretation methods and databases used to compile the basement depth estimates.

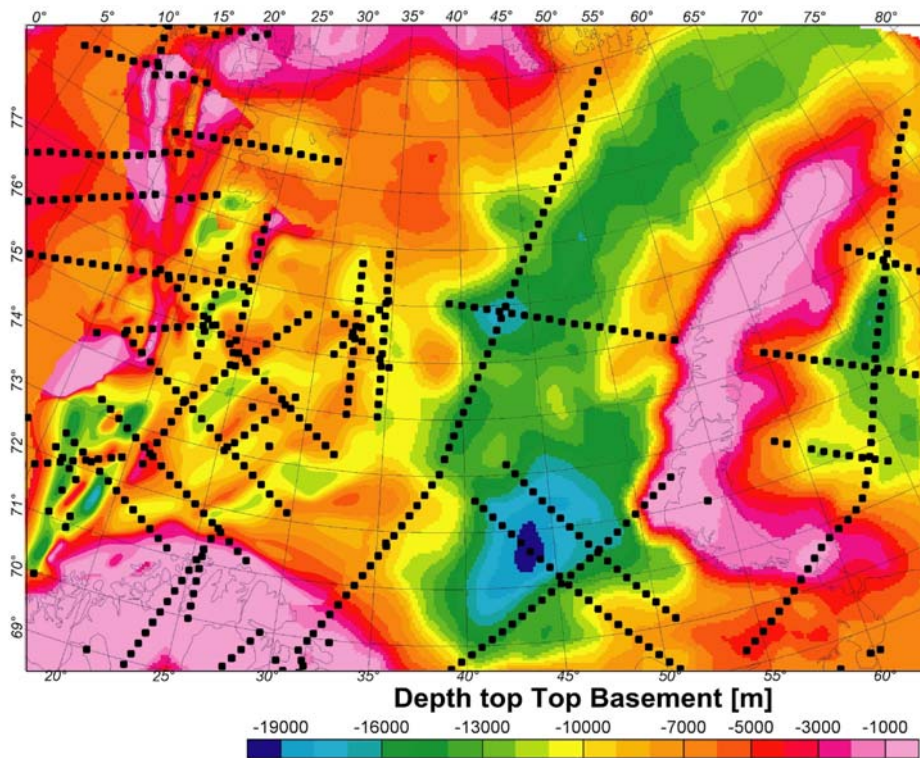
2.2 Barents50, BARMOD and Barents 3D

Barents3D (<http://www.norsar.no/seismology/barents3d>) is a hybrid 3D crust and upper mantle for the Barents Sea Region, which is a composite of two separate models, one for the crust, Barents50 (Ritzmann et al. 2007), and one for the upper mantle, BARMOD (e.g. Levshin et al. 2007).

The Barents50 model is a seismic-velocity model of the crust in the Barents Sea with a lateral resolution of 50 km (Fig. 2.3). The Barents50 model is based on 2D wide-angle reflection and refraction lines, passive seismological stations and, to a limited extent, potential field data (Ritzmann et al. 2007). The Barents50 compilation also provides information on the deep structure of the crust. For the crust, this compilation includes an intra-crustal horizon inferred mainly on the basis of velocity models and 2D gravity modelling because crustal reflectivity does not allow clear imaging from seismic data alone (e.g. Breivik et al. 2005). The seismic Moho of the Barents50 compilation is generally flat over large parts of the Barents Sea region (Fig. 2.2b). From the Atlantic continent-ocean-boundary to the west all the way to Novaya Zemlya, Moho depth varies only between 32.5 and 37.5 km. In the western Barents Sea (32.5-35 km) the depth is slightly less than in the eastern Barents Sea (35-37.5 km). The main changes can be related to the transition to Svalbard and the offshore-onshore transition to the south where the Moho rapidly becomes deeper than 40 km.

The Moho depth does not reflect observed changes in the depth to basement surface (Fig. 2a and b). From an isostatic viewpoint and simple models of crustal extension (e.g. McKenzie 1978), a correlation between crustal thickness and Moho geometry would be expected. However, in the Barents Sea the total crustal thickness appears to be generally unaffected by the processes leading to the formation of the thick basins. Only in the Kara Sea is the Moho depth locally shallower than 30 km, which indicates localized crustal thinning, but here the seismic coverage is limited and can only resolve parts of the area.

a) Depth To Top Basement



b) Depth to Moho

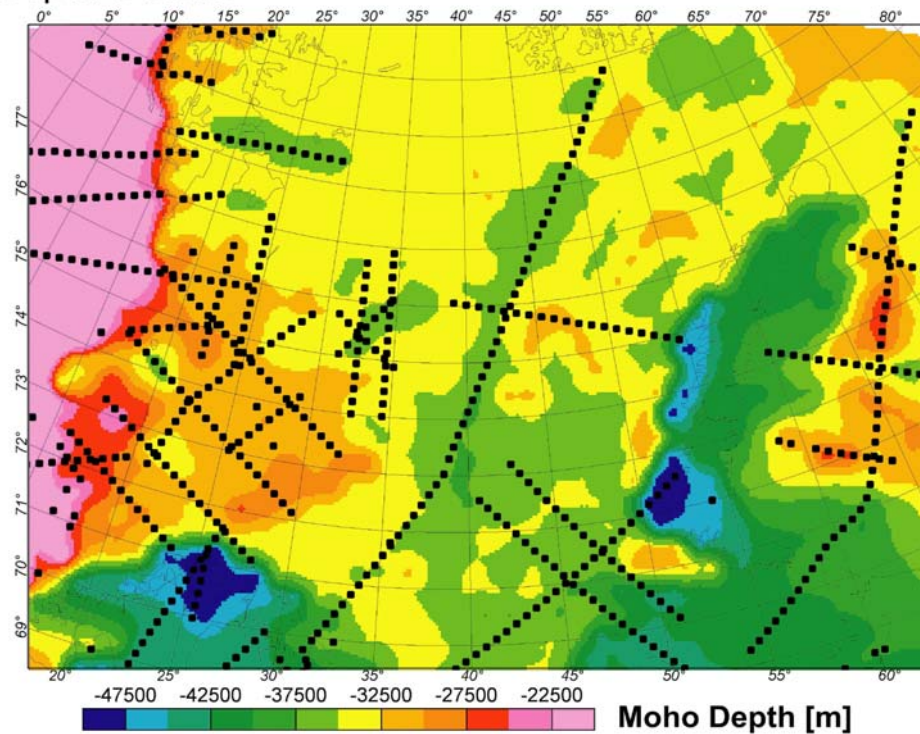


Figure 2.2 a) Depth to basement and b) depth to Moho maps. The maps are adopted from the Barents50 model (Ritzmann et al. 2007) with modifications after Skilbrei (1991, 1995) for the western Barents Sea. The black dotted lines denote the location of the regional seismic lines used in compiling the Barents 50 model.

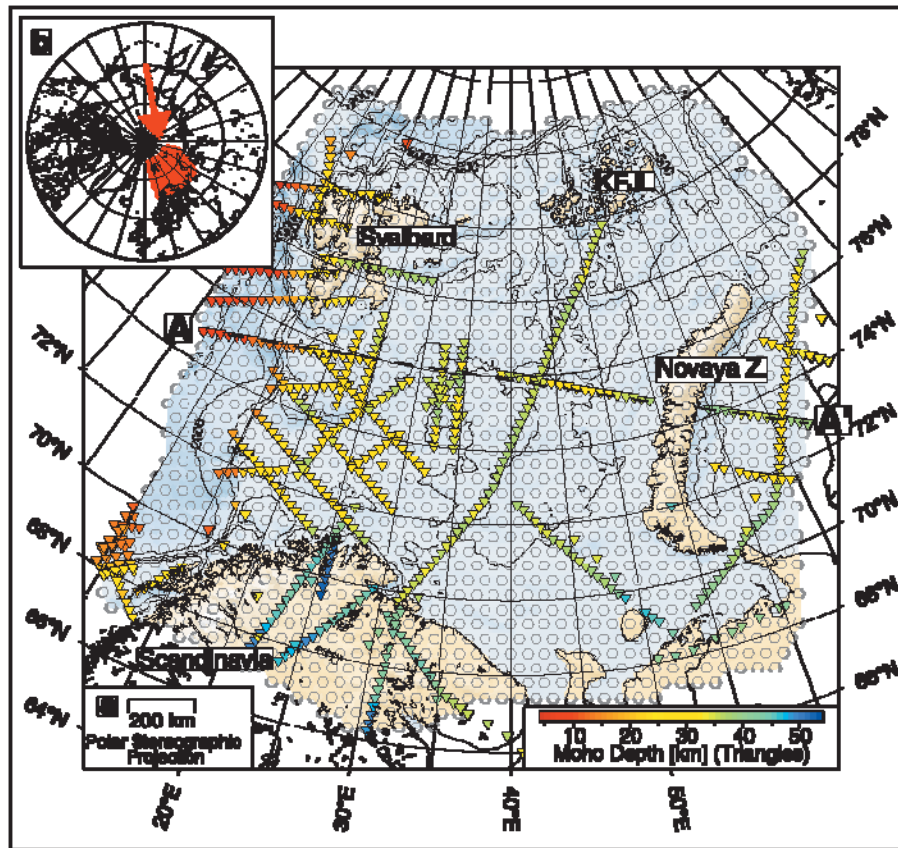


Figure 2.3 Presentation of the spatial resolution of the Barents50 and the utilized seismic profiles (in colour) (Ritzmann et al. 2007).

The upper mantle model (BARMOD; Levshin et al., 2007) is based on a large dataset of predominantly new surface-wave observations from more than 150 local and regional events with travel paths through the greater Barents Sea region. These observations of group-velocities were first inverted for 2D group-velocity maps and subsequently for a 3D S-wave velocity model with a nominal resolution of 1 by 1 degree. Applying standard conversion relations, the model contains P-wave velocities and densities.

2.3 Gravity and magnetic data

Compilations of gravity and magnetic data are available from different sources (e.g. Arctic Gravity Project 2002) and most recently from a cooperation project between NGU and the All-Russian Geological Institute (VSEGEI).

The Bouguer anomaly is calculated by removing the topographic masses and filling the water depth with a constant density. In Fig. 2.4 a reference density of 2670 kg/m^3 is used for the

land and sea areas to calculate the complete Bouguer anomaly. The Bouguer anomaly is different from previous studies as we developed a model of the ice cover over Novaya Zemlya (see Ebbing et al. 2005); something missing in previous studies (Arctic Gravity Project 2002).

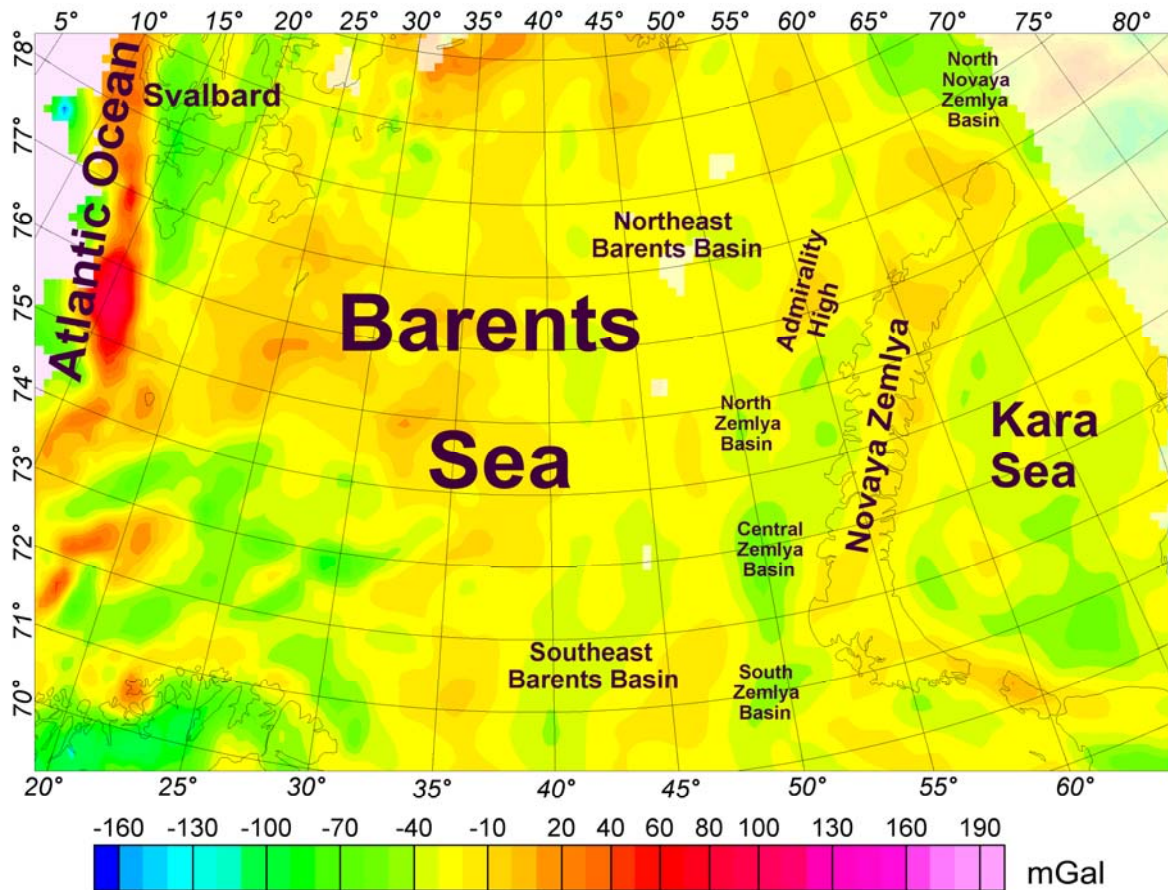


Figure 2.4 Bouguer anomaly map of the Barents Sea as compiled by the NGU-VSEGEI cooperation project (Werner et al. 2007).

NGU has covered large parts of Norwegian part of the Barents Sea and Svalbard with aeromagnetic measurements. The data sets have been described earlier (Åm 1975, Olesen et al. 1990, Skilbrei 1990). For the Russian part also a variety of surveys exists. NGU and VSEGEI compiled the available aeromagnetic datasets resulting in the anomaly map shown in Fig. 2.5. The new compilation with 5x5 km grid spacing allows a detailed view of the regional magnetic anomalies in the Barents Sea.

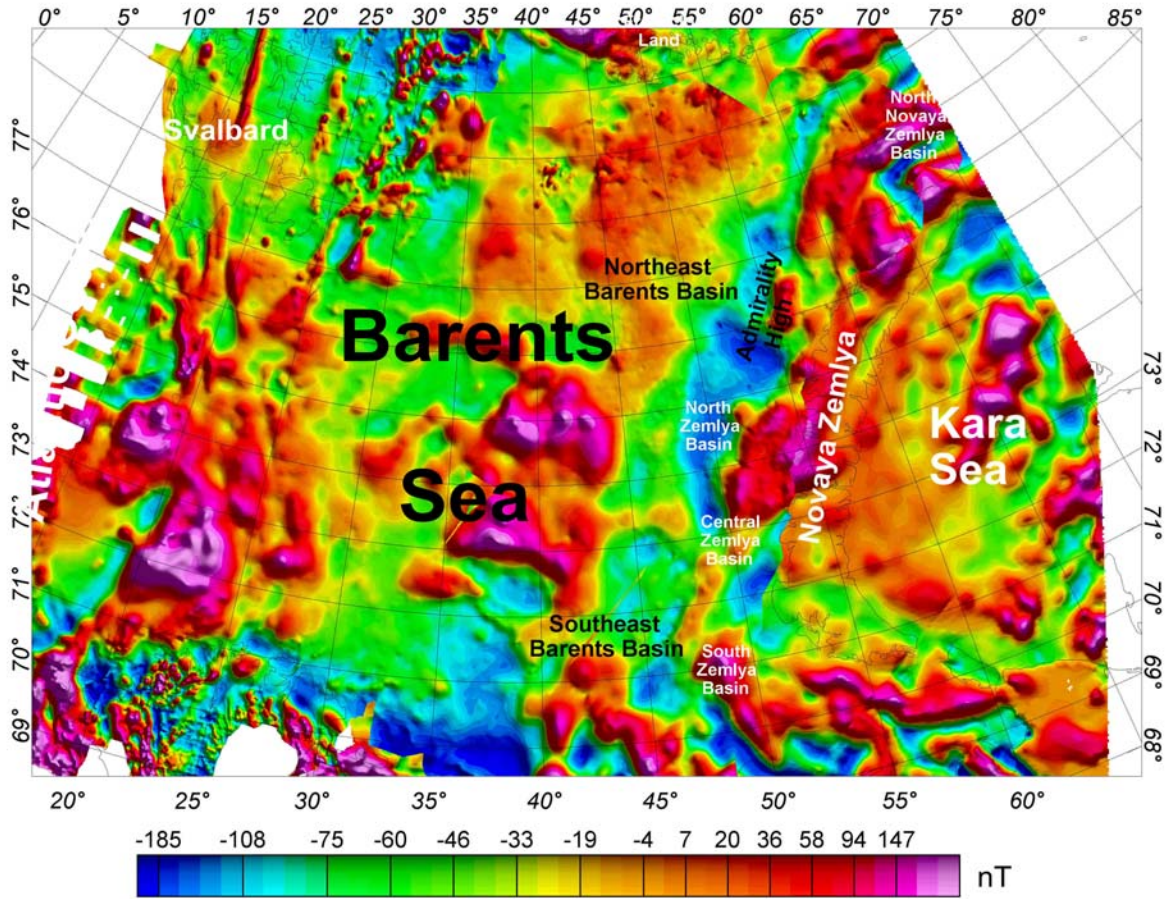


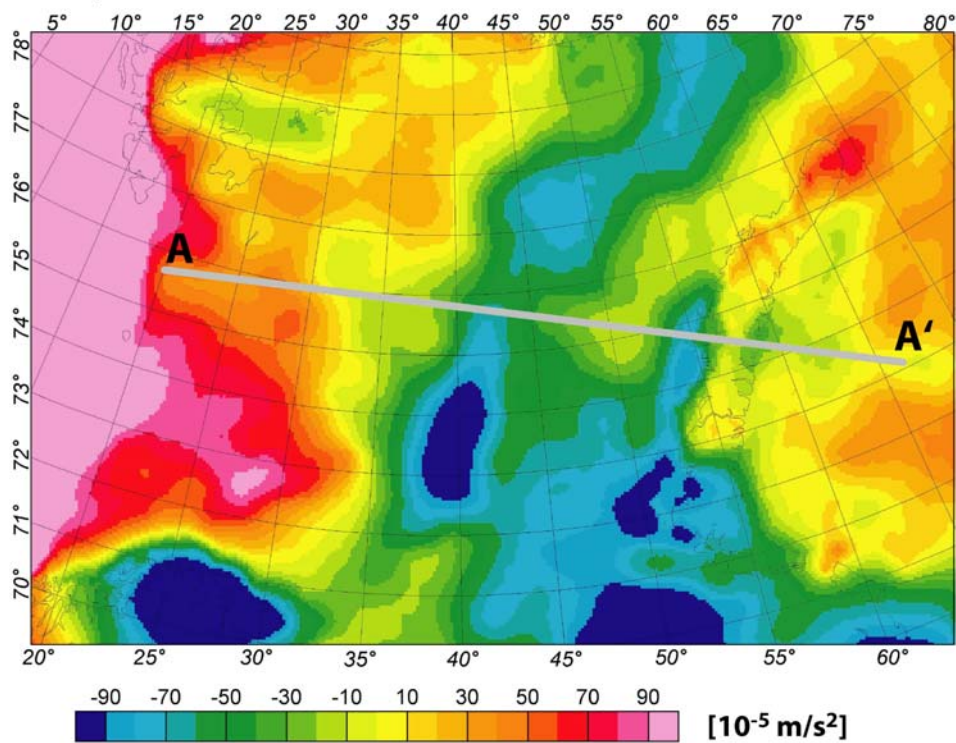
Figure 2.5 Magnetic anomaly map of the Barents Sea as compiled by the NGU-VSEGEI cooperation project (Ebbing et al. 2007b).

3 FORWARD GRAVITY MODELLING AND THE ISOSTATIC STATE OF THE BARENTS SEA REGION

The knowledge of topography, depth to basement and Moho depth (Chapter 2) allows 3D forward modelling of the crustal structure of the Barents Sea. We use the program GMSYS-3D (Popowski et al. 2006) and a normal crust reference density model (see Table 1 in Ebbing et al. 2007a). The "geological" 3D crustal model consists from top to bottom of a water layer, sedimentary rocks, crust with an intra-crustal horizon and Moho geometry from the Barents50 compilation (Ritzmann et al. 2007). For densities of the sedimentary rocks, we use a modified density-depth relationship that incorporates a sediment compaction model (e.g. Braitenberg et al. 2006, Wienecke 2006) after information by Fichler et al. (1997) and Tsikalas (1992).

The gravity effect of this 3D model is presented in Fig. 3.1 and along a profile in Fig. 3.2. In general, large differences between the observed and modelled gravity field exist, which are not constant (Fig. 3.1b). These variations mean that the offset between observed and modelled gravity anomalies cannot be adjusted by applying a constant shift value. Furthermore, the large differences and the fact that the upper crustal structure is relatively well known, suggest that the masses, needed to remove the offset, lie within the lower crust or the mantle. To distinguish between these two possibilities, we investigated the isostatic state of the model.

a) Gravity effect of 3D model



b) Gravity residual

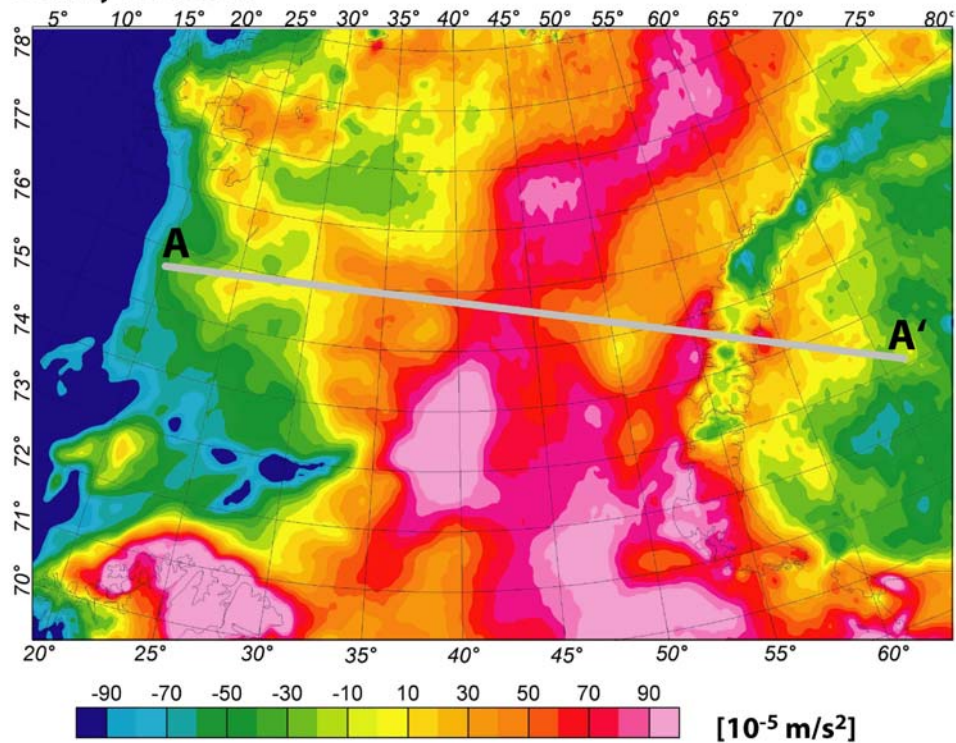


Figure 3.1 Map showing the gravity effect of the simple 3D density model based on constant densities for the crust and mantle, a density-depth relation for sedimentary rocks and geometry from Fig. 2.1. b) The residual field shows large regional differences between the gravity effect of the 3D model and the observed Bouguer gravity. The profile marked A – A' is plotted in Fig. 3.2.

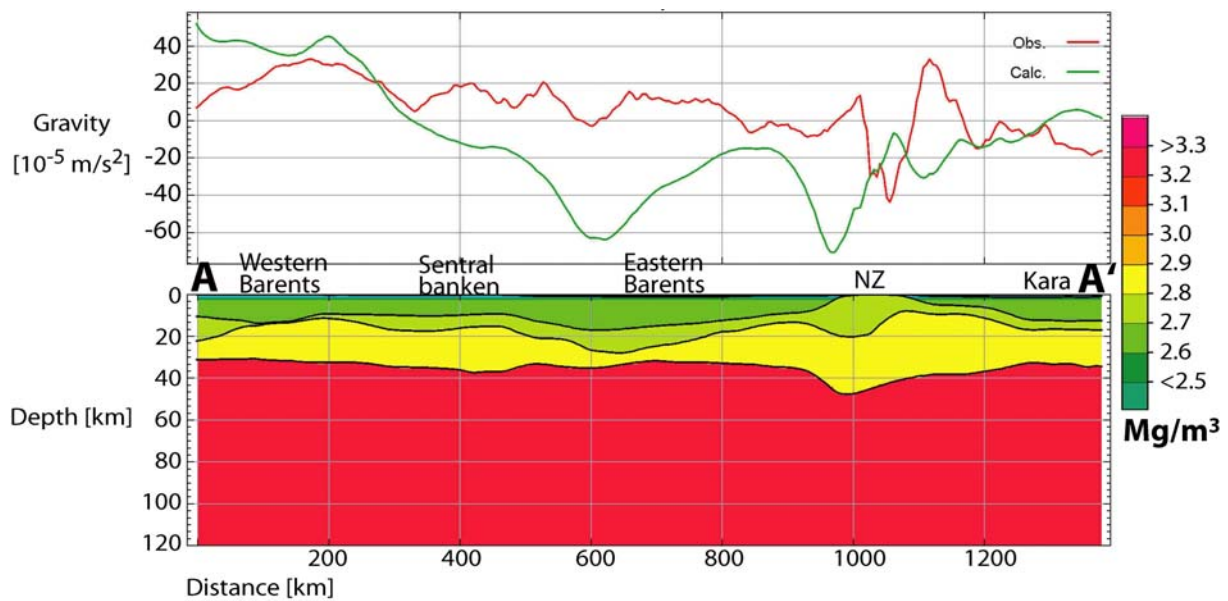


Figure 3.2 West-east profile through the model from the westernmost border of the Barents Sea to the Kara Sea showing the geometry and density distribution of the initial 3D density model. The upper panel shows the large differences between the modelled gravity effect (green line) and the observed Bouguer anomaly (red line). Profile location in Fig. 3.1.

3.1 Isostatic state of the Barents Sea Region

Isostatic compensation requires that all topographic masses (loading), and sedimentary rocks (unloading) must be compensated at lithospheric level. When the loading is zero, the Moho interface has no undulations and is located at a normal depth. In the presence of a crustal load, a flat Moho geometry corresponds either to a very high flexural rigidity, or to compensation in the mantle lithosphere. In a first approach, we consider Airy-type local isostatic compensation adjusted to take into account sediment loading. This loading is calculated using an exponential density-compaction model for the sedimentary rocks. The resulting isostatic Moho (Fig. 3.3) is very different from the seismic Moho. For example, the isostatic Moho is 8 km shallower than the seismic Moho in the eastern Barents Sea. Possible explanations for the differences are:

- (1) the applied sediment densities are too low,
- (2) there is a compensating surplus mass in the lower crust or/and upper mantle, or
- (3) the seismic Moho is too deep.

As we have constraints on the seismic Moho and the applied densities, option (2) is the most likely. Whether isostatic balance is achieved by additional masses in the lower crust and upper mantle can be discussed by considering the gravity signal.

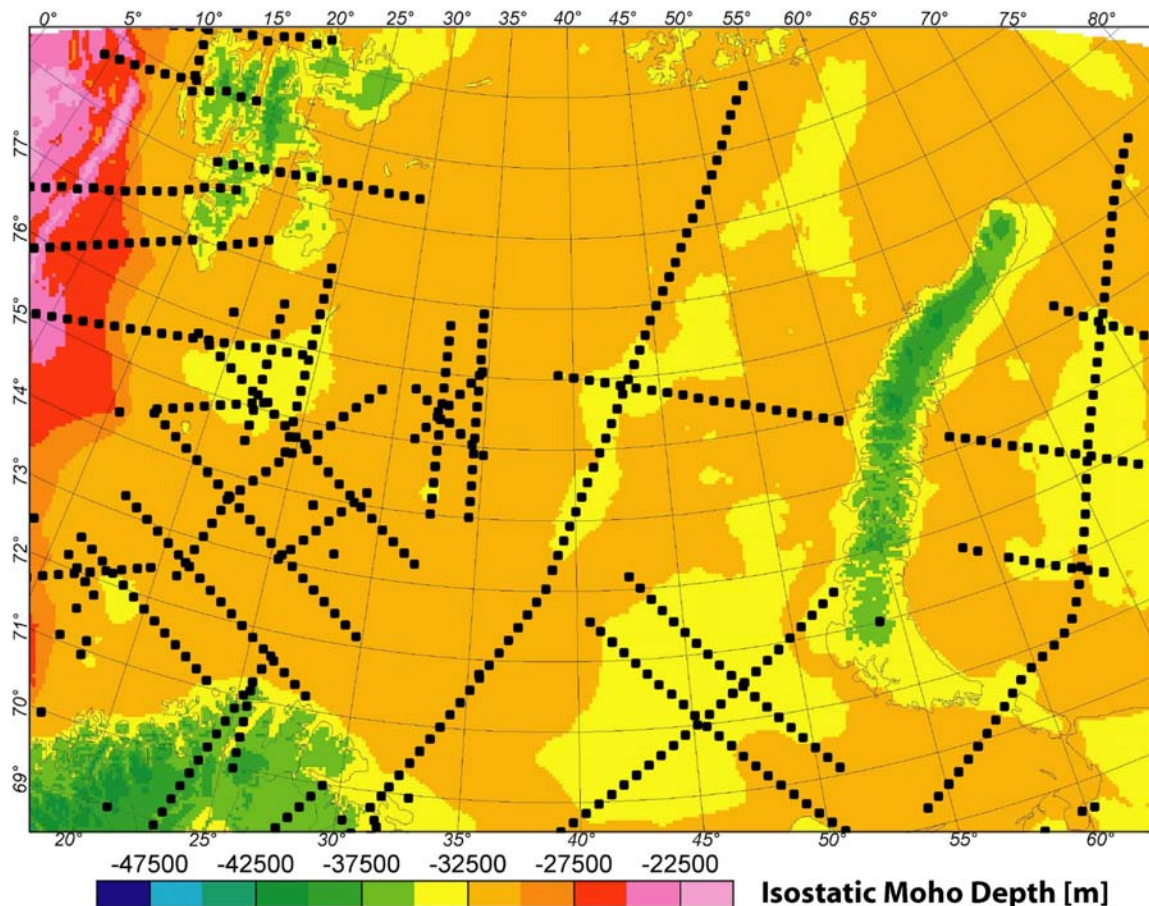


Figure 3.3 The simple Airy isostatic Moho depth (root) was calculated by taking into account the loading of bathymetry/topography and sedimentary rocks as well as a density contrast between the lower crust and upper mantle of 400 kg/m^3 and a relative normal crustal thickness of 35 km.

Flexural rigidity (which will be discussed in detail in Chapter 5) is a probable cause of deviation from local isostasy. However, accounting for the isostatic balance by flexural rigidity would not explain the observed differences in the level of the gravity field and, furthermore, would not explain the excessively deep Moho. This means that varying densities in the crust or lithospheric mantle is the only way to fit the gravity field and to account for the east-west varying discrepancy between the level of observed and modelled gravity anomalies.

The detailed concept of lithospheric isostasy and sensitivity tests for our analysis have been presented in Ebbing et al. (2005) and Wienecke et al. (2007). In short, our approach regards

the lithosphere-asthenosphere boundary, not the base of the crust, as the compensation depth for balancing the lithosphere. Hereby, local isostatic equilibrium is assumed to exist and we calculate the balance relative to a reference column. Isostatic equilibrium is now achieved by density variations in the lower crust or mantle that compensate for topographic and sediment loading. This approach of determining mass excess/deficits in the lithosphere and their associated gravity effect has been shown to be valid for regional investigations (e.g. Roy et al. 2005).

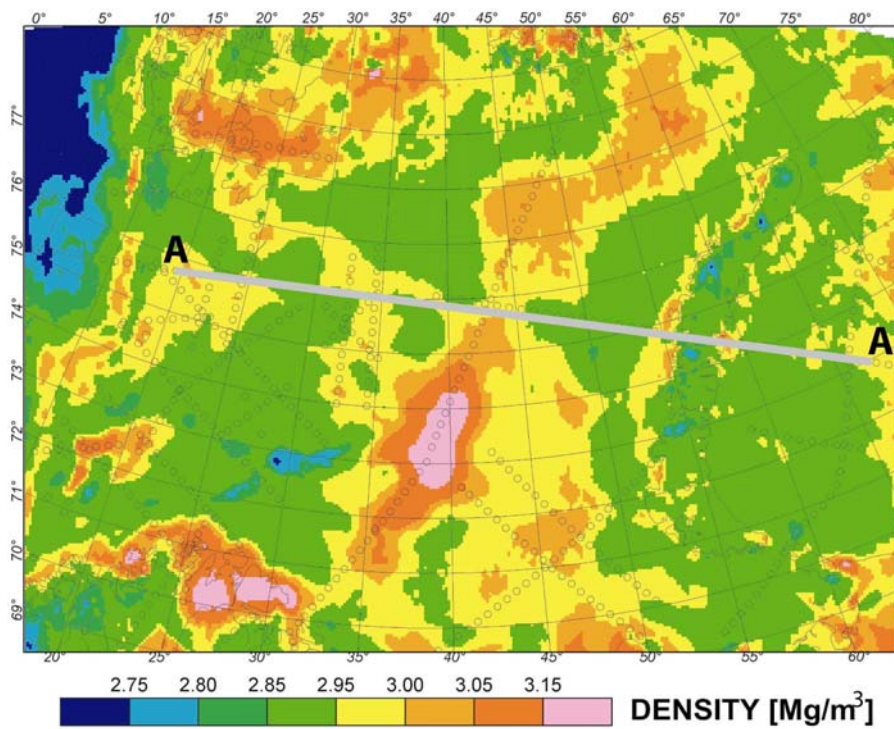
3.2 Lithospheric isostasy - results

The isostatic lithospheric mantle inversion results in densities ranging from 3250 kg/m³ to 3375 kg/m³ (Figs. 3.4b and 3.5a). Lower values are only evident for the oceanic lithosphere of the North Atlantic. Generally, the lithospheric mantle densities show a regional division between the western and eastern Barents Seas and the Kara Sea within the range of realistic density values for the upper lithospheric mantle.

Using the variable density distribution calculated for the lithospheric mantle, the large discrepancy between observed and modelled gravity is now greatly reduced (Fig. 3.6a). However, for short- to intermediate-wavelength anomalies, a substantial misfit remains. To adjust for the intermediate-wavelength anomalies, the configuration of the intra-crustal horizon of the Barents 50 model is included in the model and the density of the lower crust is allowed to vary between 2800 and 3000 kg/m³. This small variation in lower-crustal density only has a minor impact on the isostatic state (Fig. 3.4a). The changes in lower-crustal density and geometry, in addition to the isostatically calculated mantle densities, lead to an isostatically-balanced cross-section, shown along profile AA' in Fig. 3.5b, and to a reduced misfit for intermediate- and short-wavelength gravity anomalies (Fig. 3.6b).

Figs. 3.4-3.6 show the density distribution for the lower crust and upper mantle from the isostatically-balanced model of the greater Barents Sea Region. Despite the good fit between observed and modelled gravity, local differences are evident in the residual gravity anomaly (Fig. 3.6b). These can be explained by the resolution of the 3D model, which was intended to explain regional anomalies. Further adjustment would require detailed modelling of crustal structures constrained by seismic profiles.

a) Lower crustal densities



b) Lithospheric mantle densities

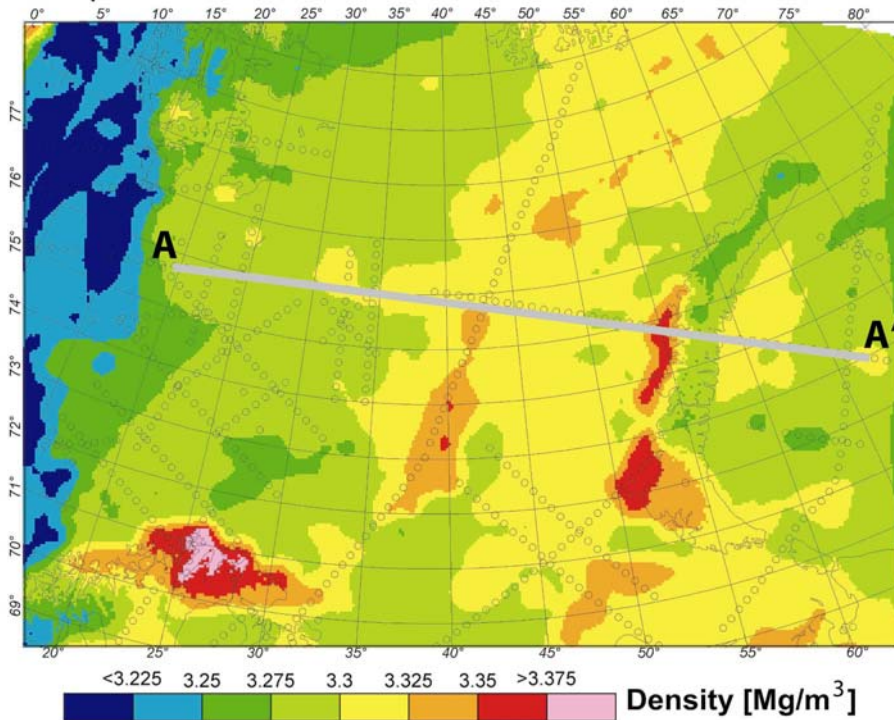
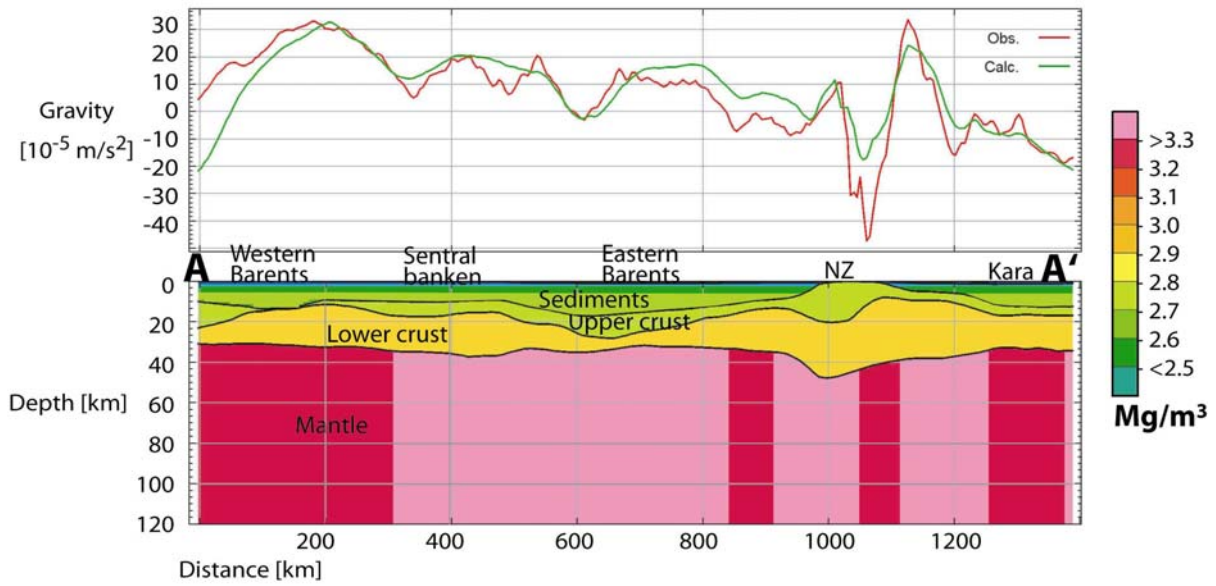


Figure 3.4 Maps showing (a) lower crustal density and (b) lithospheric mantle density variations. The varying densities allow local isostatic equilibrium to be achieved and give a modelled gravity field that fits the observed gravity to a large degree. The profile marked A – A' is plotted in Fig. 3.5.

a) Isostatic balanced



b) Isostatic balanced and gravity inverted lower crust

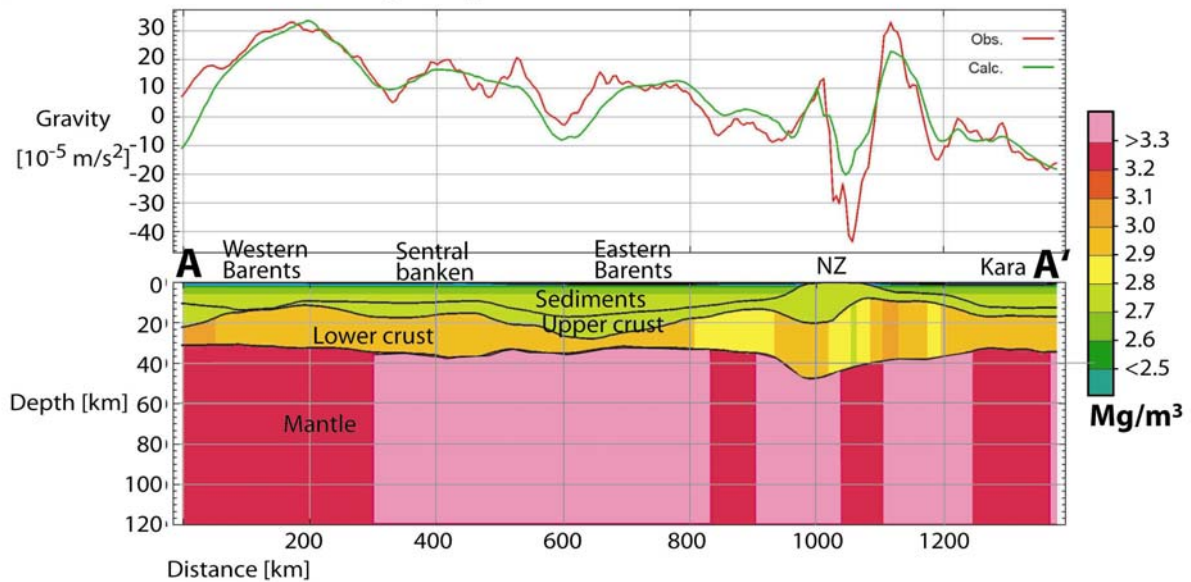
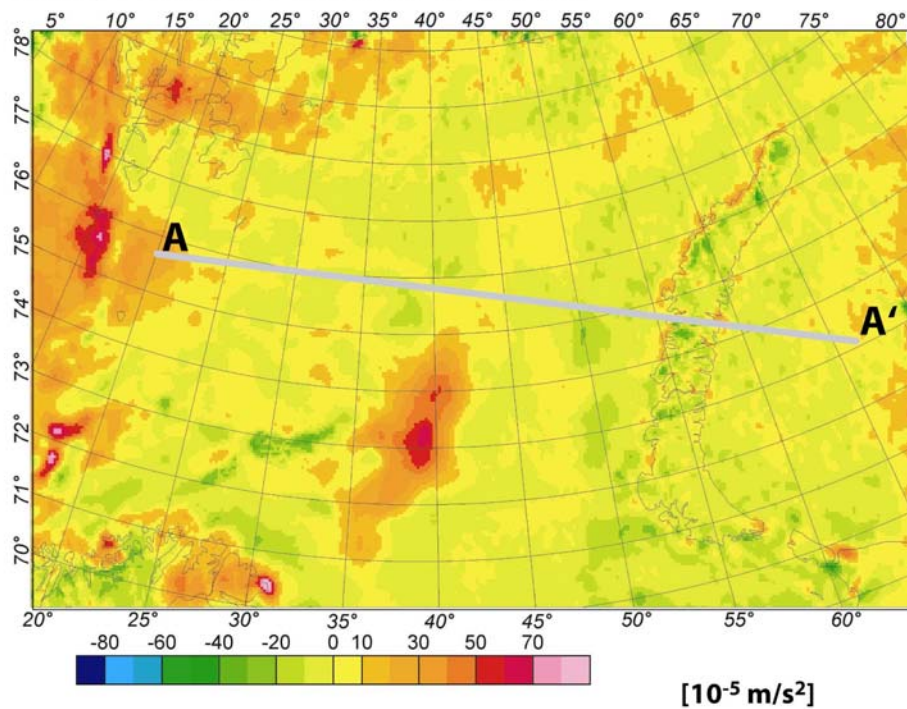


Figure 3.5 Profiles showing the same geometry as in Fig. 3.2, but in (a) the densities of the lithospheric mantle are varied to isostatically balance the lithosphere, and in (b) densities in the lower crust are also varied to reduce the misfit for intermediate- and short-wavelength gravity anomalies whilst maintaining isostatic balance. The gravity residuals of the entire 3D model are shown in Figs. 3.6 (a) and (b).

a) Gravity residual of isostatic 3D model



b) Gravity residual of isostatic and gravity inverted 3D model

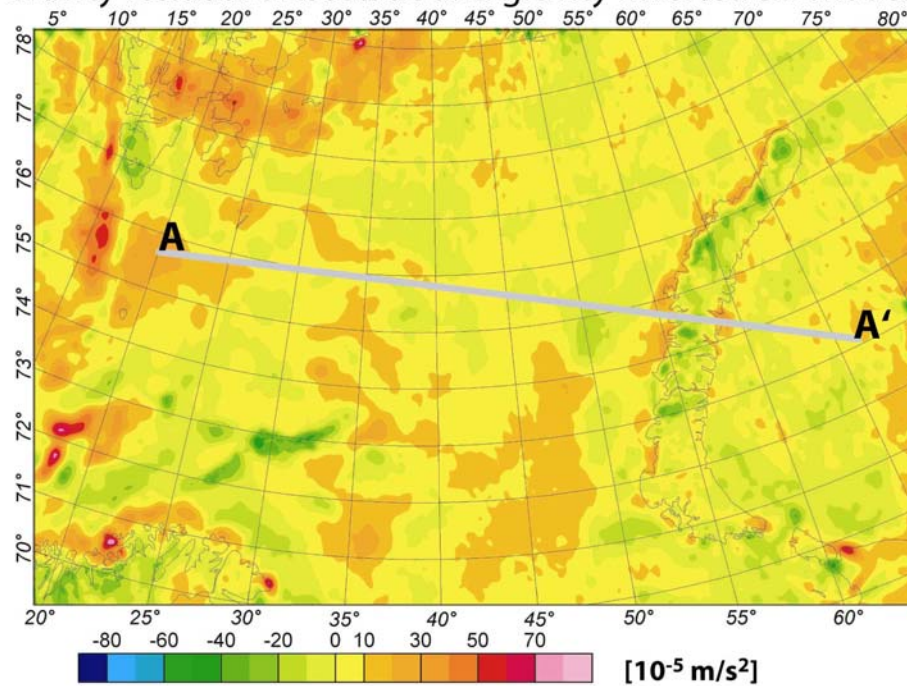


Figure 3.6 Maps showing residual gravity for the 3D models. (a) Gravity residual for the model that includes only isostatic mantle densities and the intra-crustal horizon in the computation. (b) Gravity residual for the model that also includes small lower-crustal density variations. Profile A – A' is plotted in Figs. 3.5 (a) and (b).

Different models can be tested and their sensitivity has been discussed in Ebbing et al. (2005). For example the inversion for lower-crustal density resulted in values $>3150 \text{ kg/m}^3$ for the entire eastern Barents Sea. Such a large volume of lower crustal high density material would require that the entire region is underlain by magmatic underplating or eclogites, which should be visible in wide-angle seismic data. In the Barents50 model, some areas have high velocities at the base of the crust (Ritzmann et al. 2007), but the extent of these areas is far less than indicated by the isostatic calculation. In a recent study, Ivanova et al. (2006) also commented on the strong reflectivity of the Moho related to a high contrast in seismic velocities, which is arguing against high lower crustal densities.

3.3 Comparison of mantle structure to basin outline, the geoid and upper mantle velocities

The regional density distribution in the upper mantle inferred from the isostatically-balanced 3D density model is consistent with the results of a recent seismic tomography study (BARMOD: Levshin et al. 2007). In the seismic tomography model, it can be seen that a high-velocity structure exists below the Barents Sea and deepens below Novaya Zemlya and has the appearance of a slab (Fig. 3.7). The velocity anomaly is calculated relative to a standard reference model (Dziewonski & Anderson 1981) and a thickness map of the high-velocity zone shows that the area of maximum thickness is located between the East-West Barents Sea transition zone and Novaya Zemlya (Fig. 3.8). The thickness map of the high-velocity anomaly correlates with our isostatic mantle density distribution, and also surprisingly well with the western basin boundary bending parallel to Novaya Zemlya (Faleide et al. 2006).

The changes in mantle properties correlate at the same time with areas of different basin characteristics. The deep and very wide basins of the eastern Barents Sea correlate with high lithospheric mantle densities, while the narrow (rift) basins of the western Barents Sea correlate better with low lithospheric mantle densities. This observation suggests a connection between basin formation and underlying large-scale lithospheric processes.

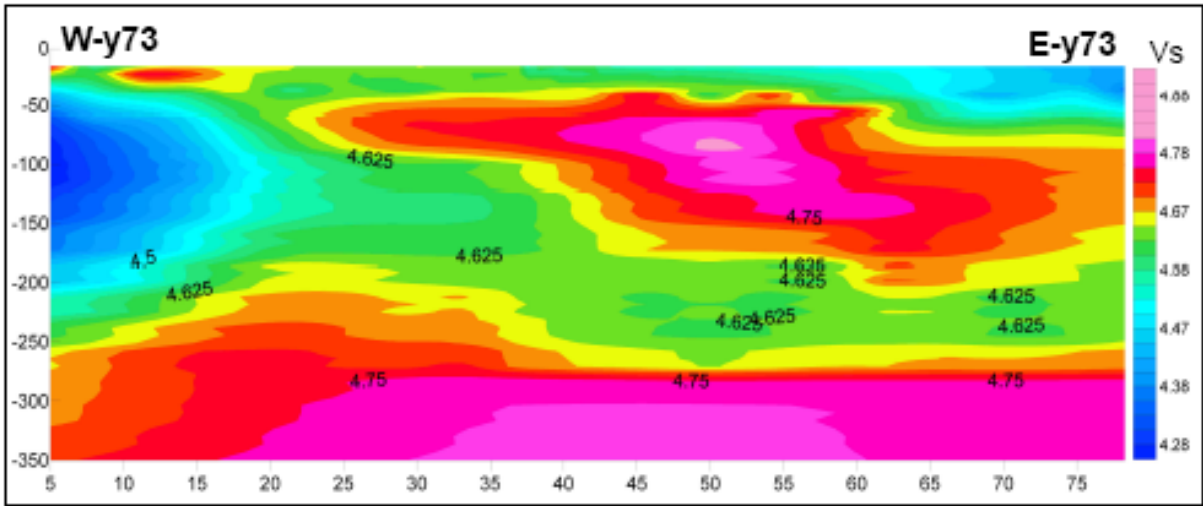


Figure 3.7 Example of the BARMOD velocity model along a west-east section at latitude 73° N. Shown are the S-wave velocities. Profile location in Fig. 3.8.

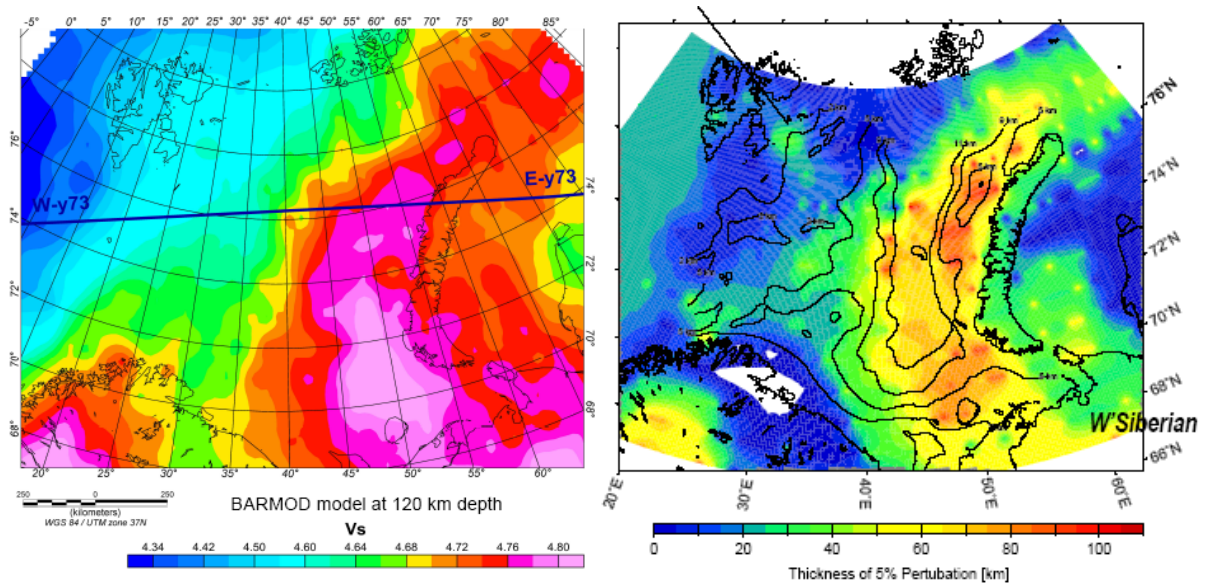


Figure 3.8 (Left) Depth slice through the BARMOD tomography model and (right) lithospheric mantle velocity perturbation (Faleide et al. 2006).

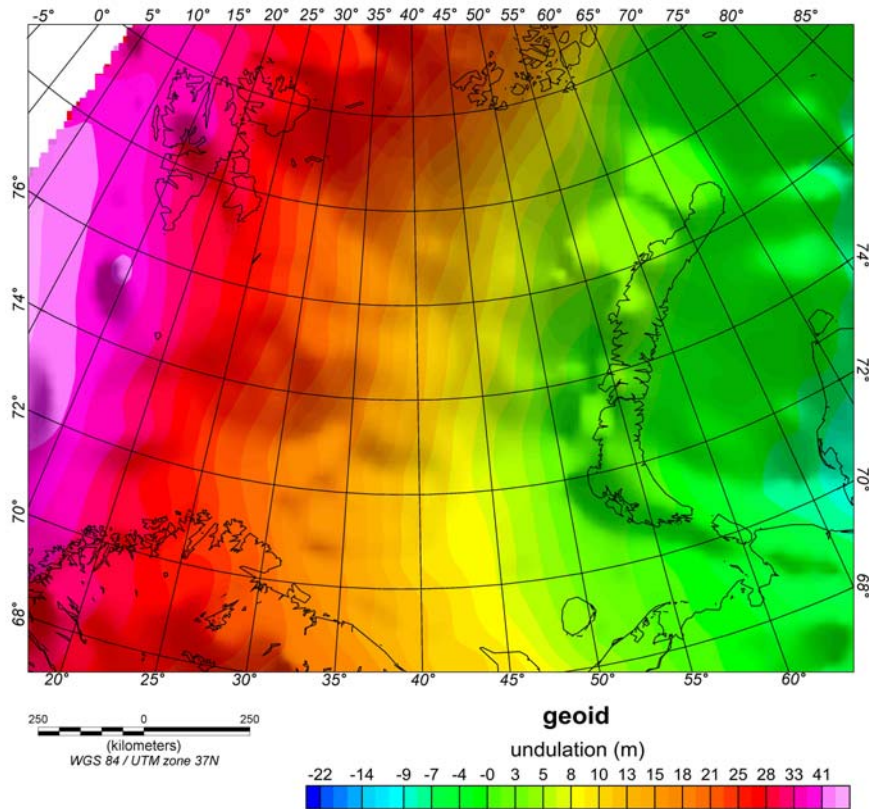


Figure 3.9 Geoid model defined from spherical harmonics to degree 360, corresponding to a wavelength resolution of >111 km (data from Förste et al. 2007).

The geoid undulation for the Barents Sea is shown in Fig. 3.9. The applied model is a combination of surface data and GRACE and LAGEOS satellite data (Förste et al. 2007), and is defined by spherical harmonics up to degree 360, which corresponds to a minimum wavelength resolution of 111 km. The geoid model contains, however, all long-wavelength components. As we are interested in anomalies in the lithosphere we calculate residual geoid undulations by removing the long-wavelength undulations that correspond to deep sources below the lithosphere. Figs. 3.10 and 3.11 show two residual fields after removing the long-wavelength components.

The residual geoid in Fig. 3.10 was computed from the spherical expressions from degree 360 to 15, corresponding to wavelengths from 111 km to 2666 km. After the removal of the ultra-long wavelength, the geoid residuals do not show an east-west gradient, but show negative values up to -3 m in the Barents Sea, and especially over the eastern part. The location of the anomaly in the eastern Barents Sea is corresponding relatively well with the high-velocity body defined from the BARMOD model.

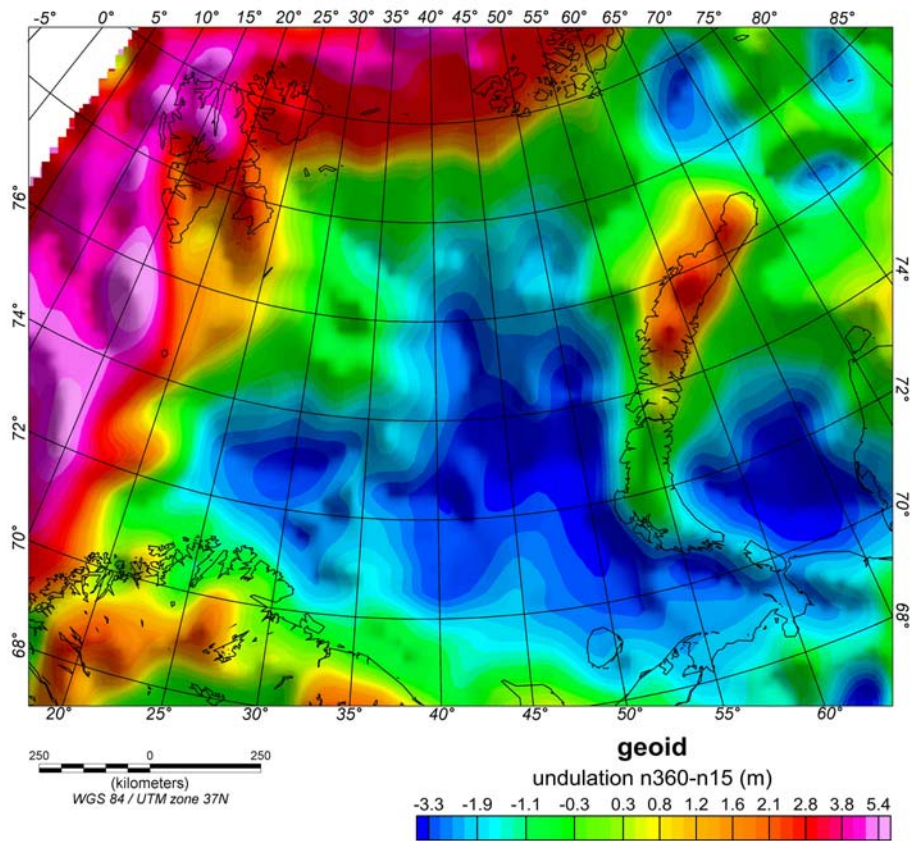


Figure 3.10 Geoid undulation defined in a wavelength range from 111 km to 2666 km.

The alternative residual geoid in Fig. 3.11 was computed from the spherical expressions from degree 360 to 20, corresponding to wavelengths from 111 km to 2000 km. This geoid residual does not feature a similar broad negative anomaly over the Barents Sea area as the first residual field. This indicates that part of the negative geoid anomaly in the eastern Barents Sea stems from a wavelength range from 2000 to 2666 km., which may still be related to long-wavelength regional features. Fig. 3.11 may, however, reflect lithospheric structures like the upper mantle density distribution and a response to the sedimentary cover in the Barents Sea. The next step should be a removal of the signal of topography and sedimentary masses from the geoid signal.

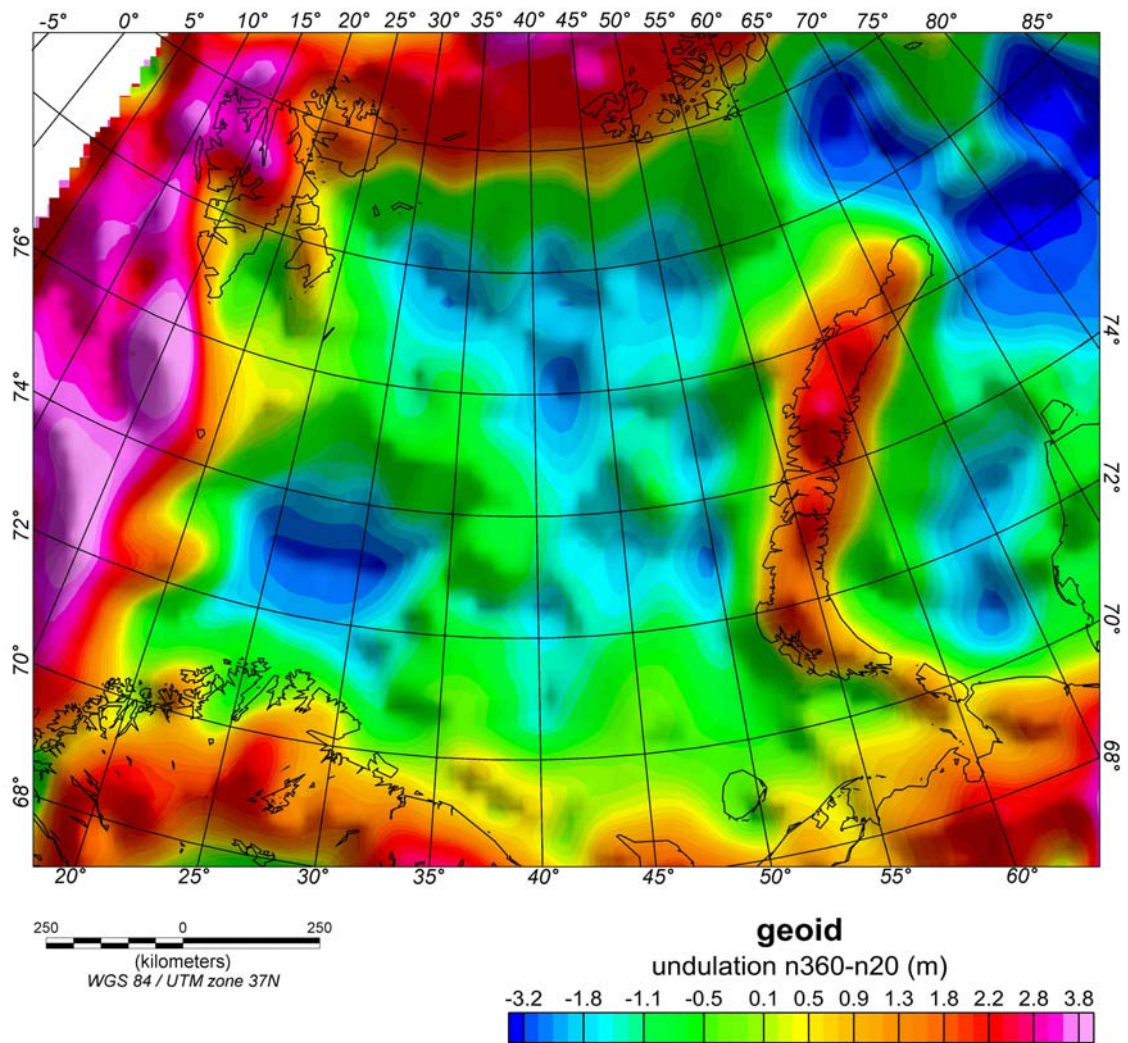


Figure 3.11 *Geoid undulation defined in a wavelength range from 111 km to 2000 km.*

As a first test, we defined a simplified 3D density model from the tomography BARMOD to calculate the magnitude of signal in the gravity field and geoid undulation for a high-density body in the upper mantle as presented in Fig. 3.8. The density variation in the upper mantle follows the outline of the seismic tomography model and we applied a density contrast of $+10 \text{ kg/m}^3$ to the high-velocity zone. Such a density contrast results in a geoid high of 11 m and a gravity effect from 10 to 44 mGal (Fig. 3.12).

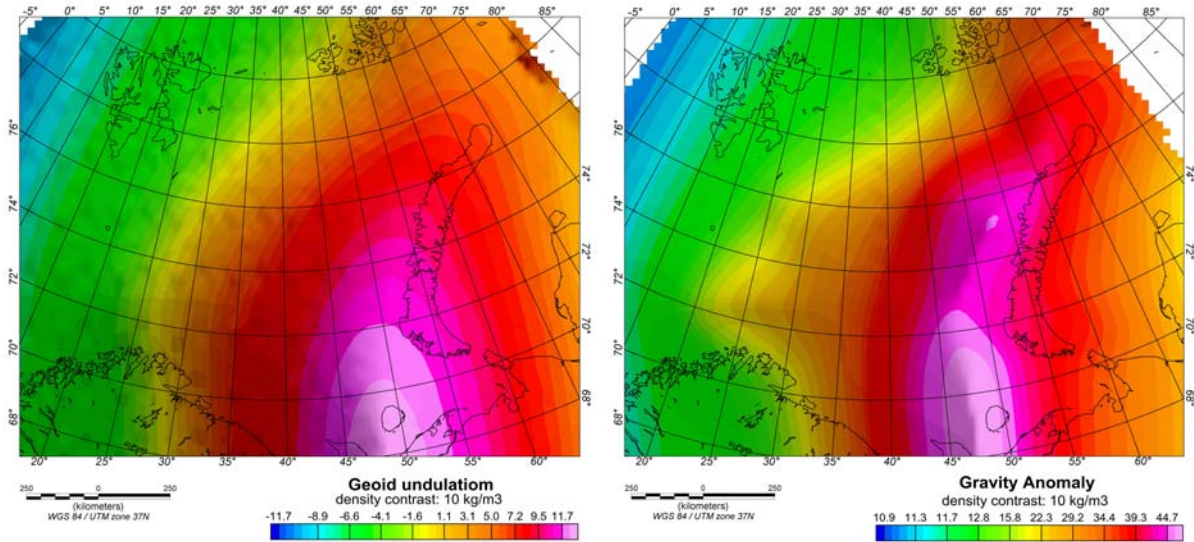


Figure 3.12 *Geoid undulation and gravity effect of the high-velocity/high-density body in the upper mantle (density contrast of $+10 \text{ kg/m}^3$ to surrounding).*

These effects are already larger than the observed anomaly, which indicates that the density contrast between the anomalous structure and the surroundings is probably too high to be realistic. In the isostatic model (Fig. 3.4) the overall density variation is in the order of 10 kg/m^3 . In conclusions, such a high-density structure in the upper mantle is plausible from the gravity signal and isostatic models, but it is difficult to present a non-unique model of the lithospheric structure applying the presently available database.

4 BASEMENT CHARACTERIZATION AND BASIN CHARACTERISTICS

The different properties of the upper mantle and lower crust in the Barents Sea are also reflected in the basin geometry and basement characteristics. Because the Barents Sea is a remote and very large area, detailed geophysical data (e.g. seismic data) are only partly available. Therefore alternative approaches must be used in order to obtain a complete picture of the tectonic framework.

The western and eastern Barents Sea contain a series of deep sedimentary basins of more than 10 km thickness with very different characteristics, when considering the wavelengths involved: the eastern Barents Sea Basins are very large whereas the western Barents Sea basins are characterised by much smaller cross-wavelengths. This observation is an indication of a different formation history of the basins which may correlate with different crustal properties.

4.1 Comparison of crustal structure to basin outline and magnetic field data

Fig. 4.1 shows the outline of basins in the Barents Sea on top of the modelled lower crustal densities. Clearly, the basins are reflected in the modelled density structure. In the western Barents Sea small-wavelength structures underlying the narrow rift basins are present, while the megabasins in the eastern Barents Sea are underlain by slightly increased lower densities. Most obvious is, however, a high-density band at the western border of the megascale basins, underlying the transition zone between the western and eastern Barents Sea.

This pattern with densities $>3000\text{kg/m}^3$ has also a strong correlation with the magnetic anomaly presented (Fig. 4.2). The magnetic field shows a major circular anomaly located at the western border of the megabasins, and a band of small-wavelength anomalies between the megascale basins in the west and Novaya Zemlya. The central Barents Sea magnetic anomaly has values >200 nT and its location and similarity in shape to the depth of top basement contours is pointing to a source in the middle to lower crust and a possible magmatic origin such as an intrusion. Similar magmatic rocks may be located at large depths below the eastern Barents Sea basin, but weakness zones at the basin flanks may have guided the migration of the magmatic material. The modelled high-densities in the lower crust might therefore be an overestimate and partly reflect upper crustal domains.

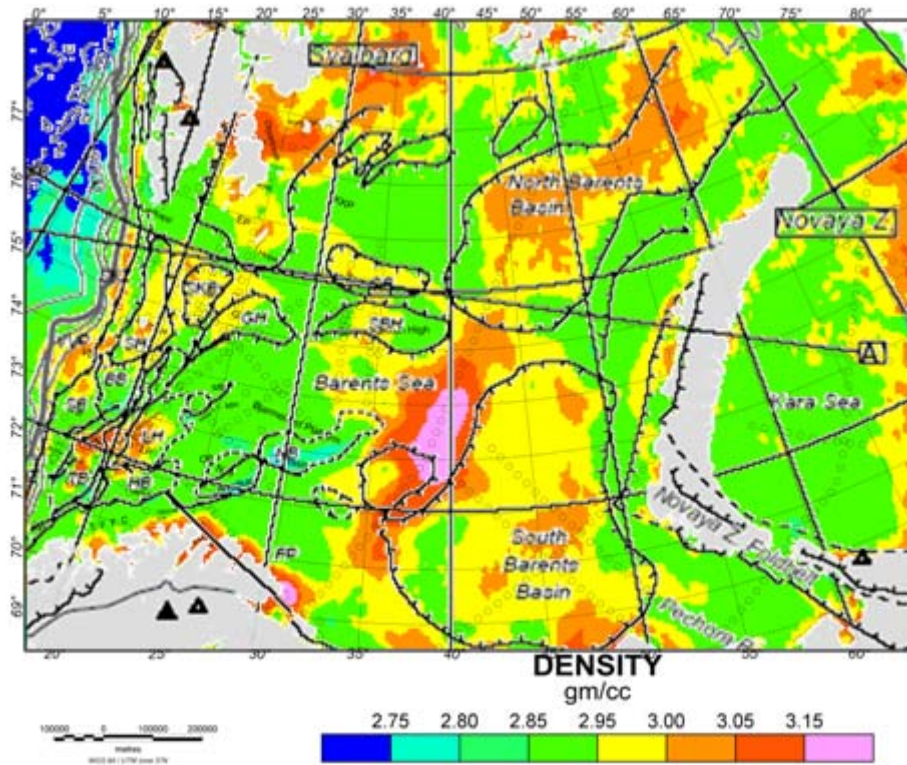


Figure 4.1 Outline of basins in the Barents Sea (after Ritzmann et al. 2007) on top of the isostatic lower crustal density distribution as presented in Fig. 3.4a

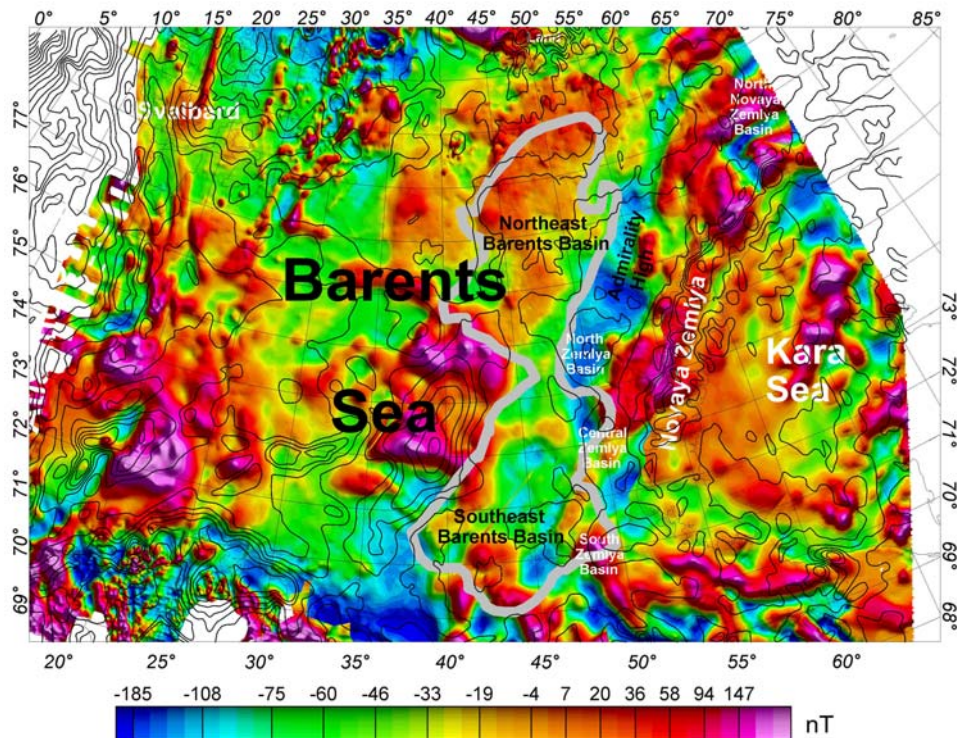


Figure 4.2 Contours of the lower crustal density distribution (Fig. 3.4a) on top of the magnetic anomaly map of the Barents Sea (Fig. 2.5). The bold grey polygon line indicates the outline of the North and South eastern Barents Sea mega-basins.

A series of magnetic highs can be observed between the Northern, Central and Southern Zemlya basins, and Novaya Zemlya, which can be caused by the shallow and partly outcropping basement.

In the western Barents Sea strong magnetic anomalies up to > 900 nT are associated with the Loppa and Stappen highs, which have already been recognized as basement highs by e.g. Åm (1975), Gabrielsen et al. (1990). Within the Loppa High region two different provinces can be distinguished from the potential field data. The western part of the basement high is characterised by a high Bouguer anomaly (70 mGal) and a medium magnetic anomaly (100 nT) whereas the eastern part is marked by a decrease in Bouguer anomaly to 0 mGal and an increase in magnetic anomaly to 900 nT. The trend of the magnetic anomalies describes an elongated half-circle and indicates a trend from the Billefjorden Fault Zone on Svalbard across the western Barents Sea into Finnmark. A comprehensive study of basement composition and the origin of the magnetic field can be found in Barrère et al. (2008) and is presented in excerpts in the next paragraph.

4.2 Western Barents Sea

For the western Barents Sea, Barrère et al. (2008) presented a characterization of the basement lithology from combined interpretation of seismic lines, gravity and aeromagnetic data. The structure of the western Barents Sea shelf has a complex history imprinted in the basement structure and lithology, and features major structural highs, platforms and basement lows (Faleide et al. 1988, 1991, 1993, 1996, Gudlaugsson et al. 1998). Using the petrophysical data from onshore Norway (e.g. Olesen et al. 1990, Skilbrei 1991, Skilbrei et al. 1991) and following magnetic lineations from onshore to the Barents Sea, a division of different basement blocks in the western Barents Sea can be made (Barrère et al. 2008).

Five different basement unit can be distinguished by comparing density, magnetisation and magnetic pattern. The transition to the eastern Barents Sea (D4 in Fig. 4.3) as well as the transition to the North Atlantic can also be identified in the regional 3D model. However, the correlation of these basement blocks with tectonic domains has to be carefully discussed.

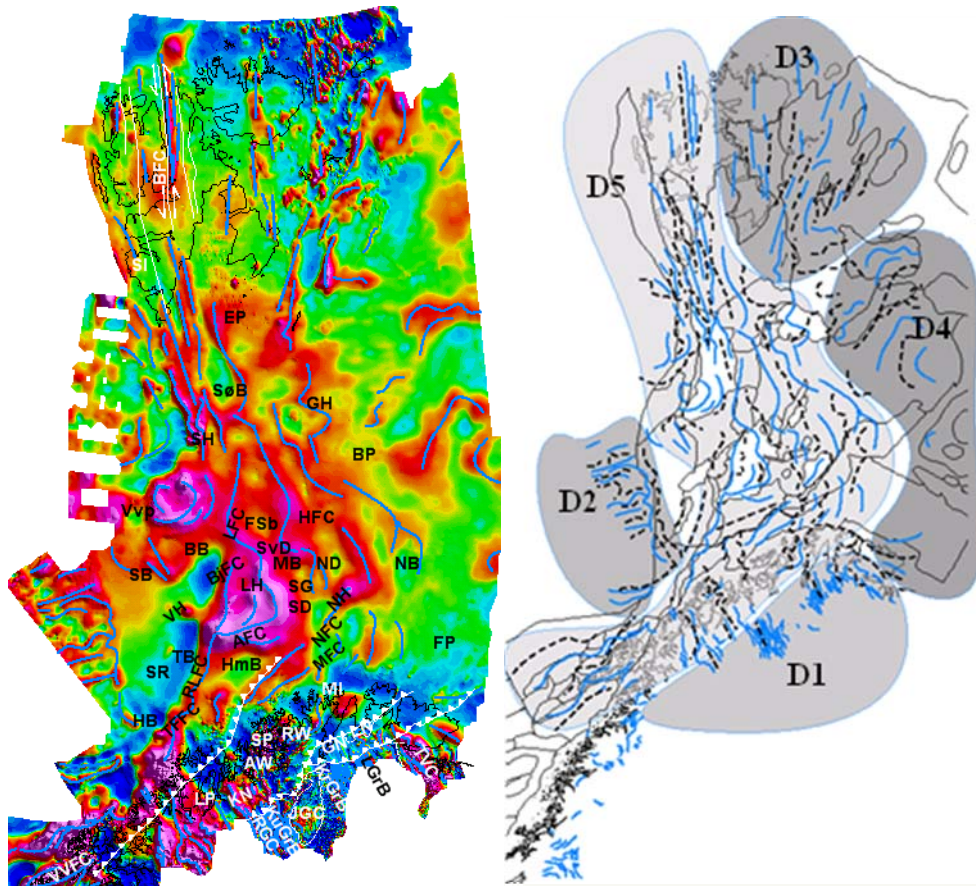


Figure 4.3 Magnetic anomaly (left) and interpretation of different magnetic domains (right), reflecting different geological provinces. Blue lines = magnetic trends. Magnetic domains: D1 - Precambrian Shield; D2- Oceanic Crust; D3- Cretaceous Volcanic Area; D4- East-West Barents Sea Transition zone; D5- Western Barents Sea basement (from Barrère et al. 2008).

4.3 Eastern Barents Sea

Our lithospheric studies show especially interesting results for the eastern Barents Sea Basins. These megascale basins with a length of up to 1400 km and a width of 550 km hold up to 20 km of sedimentary sequences and are not typical rift basins because of their large depths. Therefore, we studied other megascale basins worldwide to see if other basins feature similar unusual characteristics. Braitenberg & Ebbing (2006) describe a total of nine so-called intracratonic basins in detail, applying several consecutive steps: (1) screening of existing large-scale basins, (2) basin classification, and (3) comparison to the eastern Barents Sea. Analogies to other basins allow us to give some constraints on the evolution of the basins. We will summarize some of the main results of the study by Braitenberg & Ebbing (2006) in the following.

The presence of an underlying extinct rift and significant quantities of volcanic material for the eastern Barents Sea (Ivanova et al. 2006) justifies comparison to the Michigan Basin. The Michigan Basin and the eastern Barents Sea Basins are relatively small with regard to the geographical extension, compared to the other intracratonic basins. Clearly, for both basins the rifting process plays an important role in the early stage and/or initiation of the basin formation. However, the Michigan Basin has only a maximum sedimentary thickness of 3.5 km, while the eastern Barents Sea basins locally exceed 20 km in depth. Even with the suggested erosion in the Michigan Basin (Sloss and Scherer 1975) the total thickness is not in the same range as for the eastern Barents Sea Basins.

Continuous subsidence in the Michigan Basin is explained by free-thermal convection, which initiates pulses of subsidence (Nunn 1994). O'Leary et al. (2004) explain the subsidence histories of the South and North eastern Barents Sea basins by intermittent phases of lithospheric extension as they share the tectonic histories, at least for pre-Triassic times. Convective drawdown caused by the pulling of lithosphere toward the zone of maximum shortening, could have led to continuous subsidence. The present-day picture of the crustal structure of the eastern Barents Sea basin makes such an interpretation speculative.

Similar to the Michigan basin, the lower crust and upper mantle of the Barents Sea is interpreted to have relatively high densities. This may be associated with intrusions of hot asthenospheric material that may have metamorphosed the lower crust (eclogitisation) or were emplaced in the lower crust. If high-density material was formed or emplaced at the base of the crust the present-day geometry of the Moho may be a response to increased loading by the high-density material. As the system was becoming stable the flexural rigidity increased leading to the platform formation. This may also have caused the observed changes in vertical subsidence between the eastern and western Barents Sea.

The most prominent feature and interesting link between the shallow and deep structure in the regional transects is associated with the deep and wide East Barents Basin that formed by rapid (non-fault-related) subsidence in Late Permian-Early Triassic times. Both the timing and spatial correlation indicate that there could be a connection to Uralian collision (Ritzmann et al. 2007).

An alternative explanation is that the observed seismic Moho does not correspond to the petrophysical Moho. Rock densities depend on pressure and temperature and mineral phase transitions cause abrupt density changes and are predominantly pressure sensitive (Hartz et al. 2007). More recent basin models which account for mineral phase transitions (e.g. Kaus et al. 2005) demonstrate that modelled subsidence differs by several km when compared to results of earlier models. In a case study of the Permian to Jurassic Barents Sea scenario, Hartz et al. (2007) show how compressed lithosphere may develop deep marine basins by eclogitization (c. 10 % volume reduction) of the gabbroic lower crust, which leads to densification of the lithosphere and subsequently formation of a deep basin. Using geophysical methods, it is, however, not trivial to distinguish eclogite (crust) from peridotite (mantle). Thus, below such compressional basins the apparent Moho could be a metamorphic front within the crust below a supra-eclogite basin.

5 RHEOLOGICAL MODELLING TO IDENTIFY CONNECTIONS BETWEEN FLEXURAL RIGIDITY AND CRUSTAL STRUCTURES

The complex tectonic history of the Barents Sea is expected to have left an imprint in the basement structure and could have led to long-term changes in the mechanical and thermal structure of its lithosphere. These long-term changes may be reflected in variations in its flexural strength. The concept of regional isostasy after Vening-Meinesz (1939) proposes that the flexural strength of the lithosphere also has to be taken into account in isostatic considerations. Wienecke (2006) shows how effective elastic thickness, which is a parameter to express the flexural strength of the lithosphere, can be used to identify faults and to delineate tectonic units. The flexural rigidity D of an elastic plate is related to the elastic thickness T_e , which are related by:

$$D = \frac{ET_e^3}{12(1-\sigma^2)} \quad (\text{A4})$$

with the Young's modulus E and the Poisson ratio σ (Turcotte & Schubert 1982; see also Appendix of Ebbing et al. 2005 for more details.).

Spatial variations of T_e have in the past been identified either by working on a series of adjacent profiles (e.g. Stewart & Watts 1997 for continents; Calmant 1987 for oceans), or on a mosaic of rectangular areas (e.g. Lowrie & Smith 1994 for continents, Calmant et al. 1990 for oceans), where for each profile or area one value of T_e is fitted. The modelling of flexure is accomplished either in the spectral domain or in the spatial domain. The data that are used in the calculations are generally the gravity field, the loads caused the topography or bathymetry, and crustal density inhomogeneities.

Wienecke (2006) developed a unified Analytical Solution for the Elastic Plate (ASEP), which can be used to solve the flexure equation for an elastic plate by inversion. If available, additional geophysical constraints can be used in the modelling, as e.g. seismic lines in order to constrain the amplitude of a subsurface load, by comparing the observed basement depth with the predictions from the flexure model (e.g. Braitenberg et al. 2002).

An alternative approach is the determination of the elastic thickness by forward modelling (e.g. Buitter et al. 1998). The flexure equation is solved numerically (here with the finite difference method) for several T_e distributions and the calculated deflection of horizons (e.g. basement or Moho) is fitted to observations with a root-mean-square norm. Forward and

inverse modelling techniques, if using the same input data, should result in the same prediction for T_e . In this chapter we compare and discuss the flexural strength of the Barents Sea lithosphere from forward and inverse modelling.

5.1 Inverse flexural modelling with ASEP

The elastic thickness in Fig. 5.1 has been calculated by Wienecke et al. (2007) using available information about topographic loading as well as crustal internal loading, which have been taken directly from the Barents 3D velocity model. The resulting elastic thickness distribution in the Barents Sea shows large differences between the eastern and western Barents Sea (Fig. 5.1). Towards Svalbard in the north-west and over Novaya Zemlya low values are calculated, indicating a weak lithosphere. High T_e -values >55 km are resolved for most of the Barents Sea.

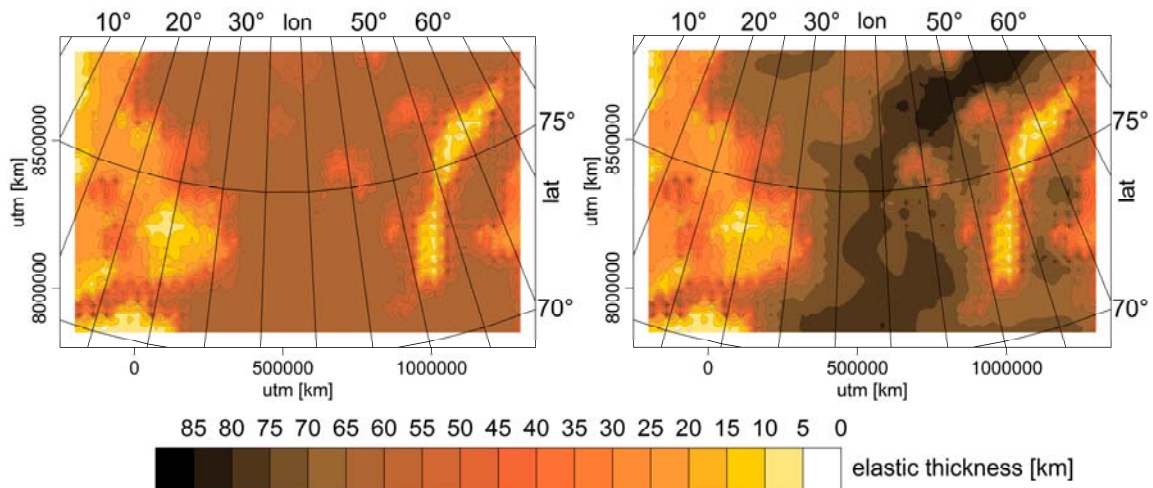


Figure 5.1 On the left side: elastic thickness distribution calculated with the ASEP and constant Young's modulus of 100 GPa. On the right side: elastic thickness distribution calculated with the ASEP and Young's modulus variation shows high elastic thickness values variation in the middle part of study area (40 longitude) (from Wienecke et al. 2007).

Wienecke et al. (2007) refined the elastic thickness calculation by using information about the Young modulus as calculated from seismic velocities of the Barents3D model. The central part of the study area, the transition between western and eastern Barents Sea, is characterized by very high elastic thickness values >60 km, which correlates surprisingly well with the basin outline and the distribution of mantle densities and velocities.

In summary, the study area in the Barents Sea is characterized in the western part by relatively small elastic thickness values and rift-type sedimentary basins, while the eastern part is characterized by high T_e -values and large-scale intra-cratonic basins. These results correlate well with the structural setting of the Barents Sea and other data sets, e.g. basement depth, basin outline. However, these preliminary results must be carefully evaluated, as the information contained in the Barents3D model was compiled with hindsight to seismological purposes and internal inconsistencies exist especially in the central part of the Barents Sea (Ritzmann et al. 2007, Ritzmann pers. com.).

The applied loading in the calculation does furthermore not adjust the gravity field in the Barents Sea Region and large residuals exist. An option to explain the residuals is with isostatic consideration as presented in Chapter 4. Alternative, more sophisticated velocity-density conversions have to be applied which consider the pressure, temperature and composition of the crust in the Barents Sea, to generate a model consistent with the observed gravity and seismic velocities.

5.2 Forward numerical modelling

Buiter (2007) evaluated the effective elastic thickness of the Barents Sea region by forward calculation of lithospheric flexure under the loads of water, sedimentary layers and optionally intracrustal loads. These loads are compensated by the strength of the crust and lithosphere in a local (Airy isostasy) or regional (flexure) manner.

Calculations of elastic thickness have been carried out made along two profiles from south of Svalbard to Novaya Zemlya considering the following alternative compensation mechanisms:

- 1) Local compensation by Airy isostasy.
- 2) Flexure of an elastic plate (for variations in T_e).
- 3) Flexure of crust and lithosphere with a depth-dependent rheology (for variations in rheology).

The results of the numerical modelling (Figs. 5.2-5.4) show that the present-day loads of water and sediments in the Barents Sea region are almost entirely compensated by local Airy isostasy or a very thin elastic plate. The two profiles are therefore in local isostatic equilibrium which agrees with the results of the density modelling (Ebbing et al. 2007,

Chapter 3 this report). The crust of the Barents Sea is thus weak from an isostatic point of view.

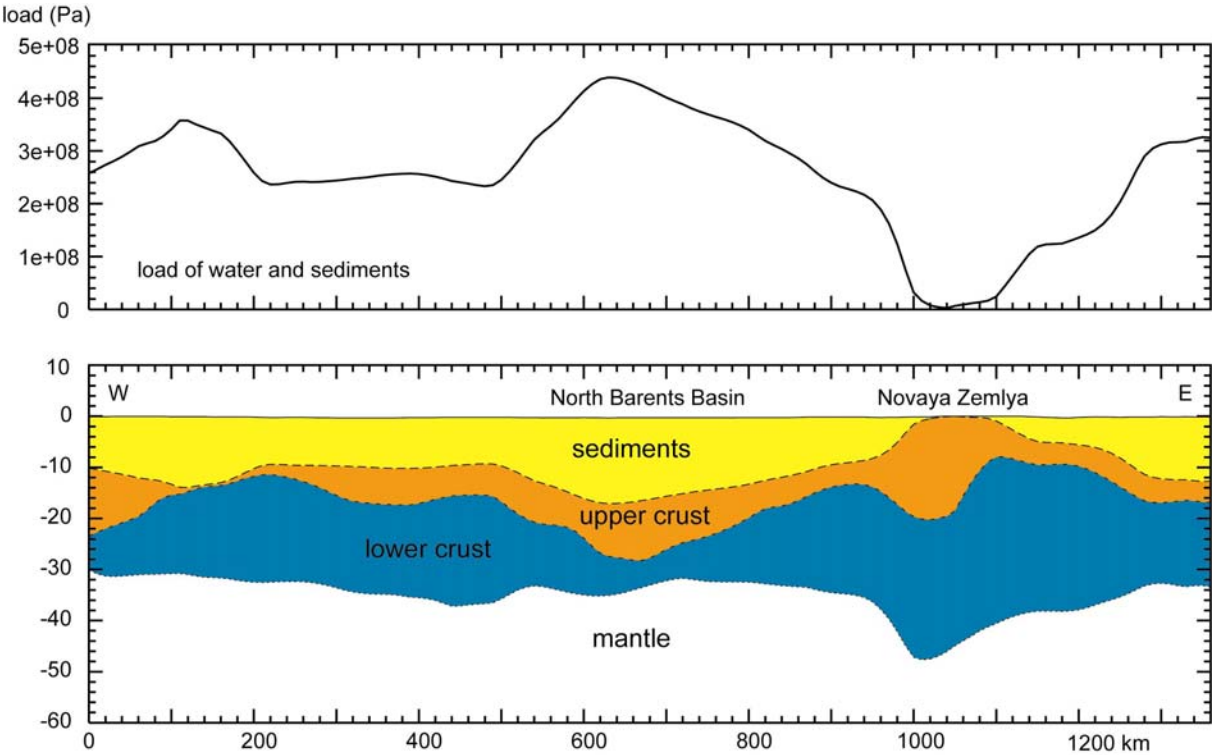


Figure 5.2 Thickness of the crust and sedimentary cover along Profile 1 (see Fig. 2.1 for location), after Ritzmann et al. (2007) and (above) the vertical load exerted by the water and sedimentary layers.

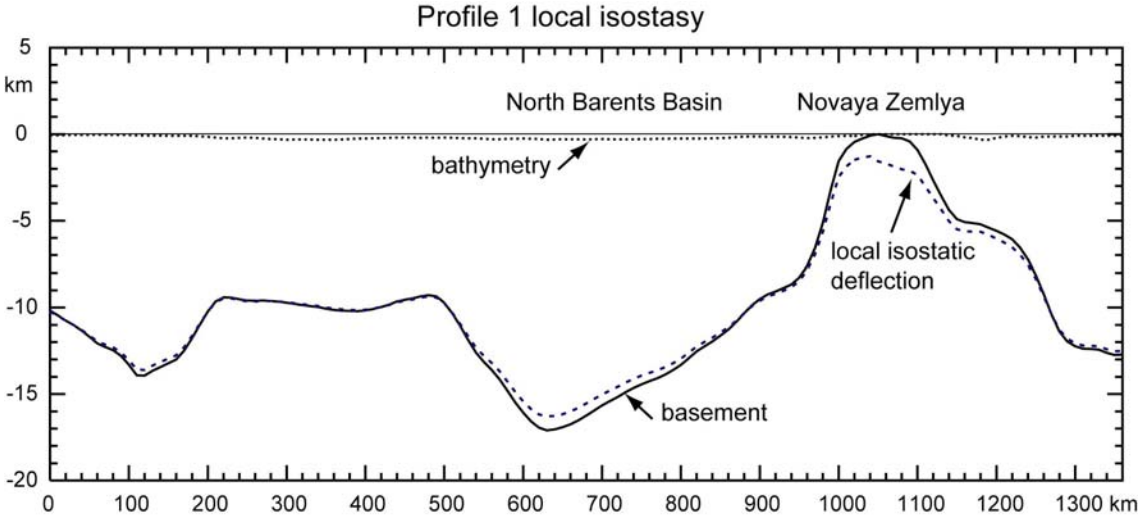


Figure 5.3 Airy isostatic deflection compared to basement depth along Profile 1. Density of mantle is 3300 kg m^{-3} , the density of the sedimentary rocks is depth-dependent (an average of 2600 kg/m^3 is adopted) (Buiters 2007).

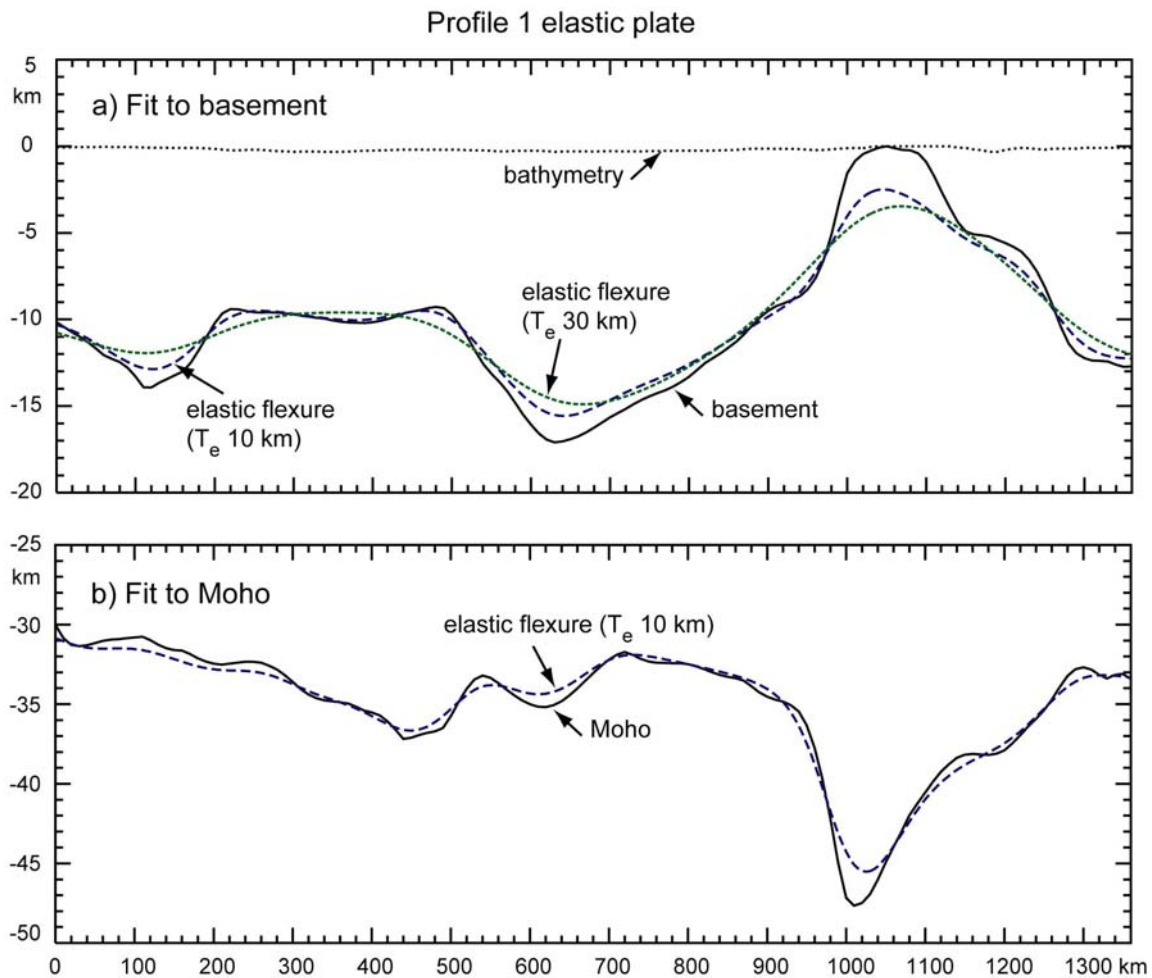


Figure 5.4 Flexure of a thin elastic plate along Profile 1. a) Deflection of plates with elastic thickness 10 and 30 km compared to basement depth. The elastic plate is loaded by water and sediments b) Deflection of an elastic plate with thickness 10 km compared to the Moho. The plate is loaded by water, sediments and crustal density differences (Buiter 2007).

The difference in width and depth of the sedimentary basins between the western and eastern Barents Sea is not reflected in a difference in effective elastic thickness. Furthermore, lateral variations in effective elastic thickness are not needed to explain the main features of the basement deflection.

5.3 Discussion of elastic thickness estimates

The results of the calculation by Buiter (2007) are in clear contrast with Wienecke et al. (2007) who show low values for elastic thickness in the west Barents Sea and high values throughout the central and eastern Barents Sea. Synthetic tests (Buiter 2007) show that the two modelling methods (forward finite difference of Buiter 2007 and ASEP of Wienecke et

al. 2007) give the same solution to a simple problem and are both robust. However, they result in different solutions for the Barents Sea area, with ASEP leading to higher values for the effective elastic thickness than the forward modelling method. A reverse test in which the T_e solution of ASEP is used in the forward modelling method shows that the ASEP solution is too stiff and does not result in a good fit to the Barents Sea basement deflection (Buitert 2007).

Buitert (2007) further argue that the ASEP solution may need a stiff plate to compensate for additional loads that were applied. This points to a conceptual difference in the modelling techniques as explained in Figure 5.5. The ASEP model has a reference Moho at 30 km depth, which is too shallow for the Barents Sea region. A reference Moho which is shallower than the average Moho for an area generates artificial upward directed forces. These extra forces need to be compensated by an increase in plate stiffness, because otherwise upward bending would result. A second difference is that the calculations by Buitert (2007) are based on information from a 3D density model that is adjusted to explain the gravity field of the Barents Sea. The density distribution used by Wienecke et al. (2007) stems directly from parameters given by the Barents3D seismic model, and the misfit between the gravity effect of the applied density distribution and the observed gravity field is of the order of up to 200 mGal. These large differences point towards a need for an adjusted density distribution and hence different loading. In addition, a modified density structure and consequently velocity structure, would also affect the Young modulus distribution in the Barents Sea.

To progress, velocity-density conversions which account for the pressure, temperature and composition of the crust in the Barents Sea, have to be established to generate a model consistent with the observed gravity and seismic velocities. Here, also input from petrophysical models is crucial. An adjusted 3D model is currently under development within the frame of the PETROBAR project, which will allow a recalculation of the results obtained with the ASEP for the Barents Sea Region.

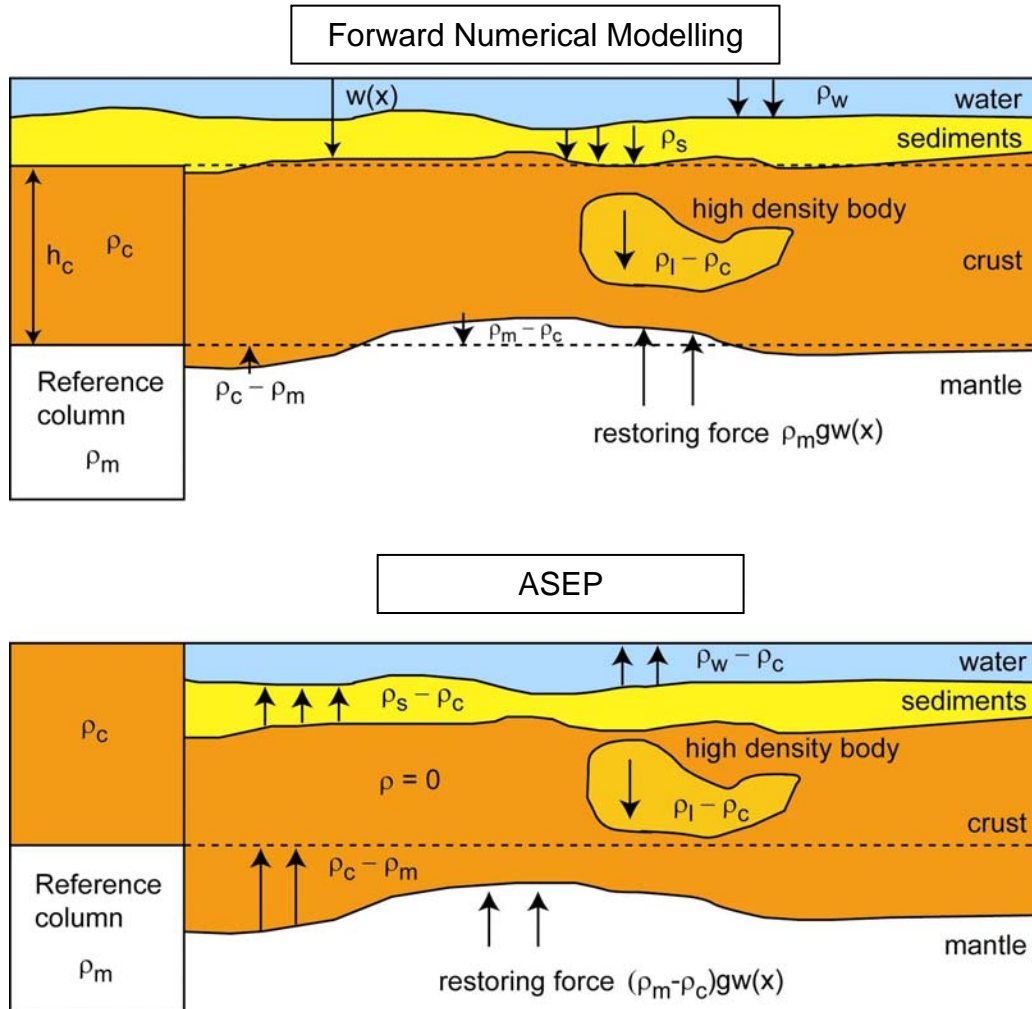


Figure 5.5 (top) The forward model applied in Buiter (2007) uses the full load of the water and sedimentary layers to calculate the basement deflection. If the deflection of the crust-mantle interface is calculated, the loads caused by lateral density and thickness changes in the crust are also taken into account. The crustal reference column then uses the average crustal thickness along the profile (e.g., $h_c = 24.9$ km along profile 1). (below) The ASEP method used by Wienecke et al. (2007) refers all densities, including those of the water and sediment layers, to a reference column. In the Barents Sea area, Wienecke et al. (2007) use a crustal thickness of 30 km. However, the crust-mantle interface in the Barents Sea area is on average deeper than 30 km in the Barents Sea area

6 DISCUSSION AND OUTLOOK

Gravity forward modelling and isostatic considerations clearly show that the lithospheric mantle below the Barents Sea Region is not homogenous (Ebbing et al. 2005). The regional density distribution in the upper mantle inferred from the isostatically-balanced 3D density model is also consistent with the results of a recent seismic tomography study (Levshin et al. 2007), and especially the thickness map of a high-velocity mantle (Faleide et al. 2006).

The changes in mantle density also correlate with areas of different basin characteristics. The deep and very wide basins of the eastern Barents Sea correlate with high lithospheric mantle densities, while the narrow (rift) basins of the western Barents Sea correlate better with low lithospheric mantle densities. This observation suggests a connection between basin formation and underlying large-scale lithospheric processes. In a similar study of the eastern Colorado Plateau and the Rio Grande rift, Roy et al. (2005) showed such a connection between upper mantle structure and tectonic provinces. Changes in mantle densities may also reflect the presence of different plates and/or different lithospheric ages. A proposed west-east-trending Caledonian suture crossing the entire Barents Sea (Gee 2004; Breivik et al. 2005) would fit with this scenario. However, the distribution of lithospheric densities is inconsistent with the presence of a Caledonian suture to the east of the Central Barents transition because the suture would crosscut the area of high-lithospheric-mantle density.

However, such a suture would be reflected mainly in the crustal composition. The density distribution in the lower crust shows relatively high densities along the transition between the western and eastern Barents Sea as well as a prominent change in the intra-crustal horizon (Fig. 3.5) and large gravity residuals that remain after including only the isostatic mantle densities in the gravity model (Fig. 3.6a).

Our observations suggest a possible relation of the East Barents Sea basins to the Neoproterozoic Timanide Orogen of eastern Baltica (e.g. Gee & Pearse 2006). If the mantle densities are related to the Timanide Orogen, the tectonic setting of the eastern Barents Sea must have been very stable since the Neoproterozoic and less affected by the Caledonian orogen than previously assumed. This would imply that a suture zone could exist between the eastern and western Barents Sea related to this ancient tectonic process.

The deviation from McKenzie-type isostatic equilibrium, the high-density upper mantle densities, and the relatively flat and deep Moho observed in the eastern Barents Sea by seismologic investigations are apparently properties which are typical of large-scale (intracratonic) basins. Analysis of the isostatic state can thus be used for distinguishing between basins formed in a extensive stress regime (e.g. rifting) from the basins formed by the interplay of vertical forces due to a combination of heating and loading.

The stable setting of the eastern Barents Sea compared to the western Barents Sea can also explain the presence of the deep intra-cratonic basins. The mantle densities may indicate different tectonothermal ages of the plates or changes in the gravitational potential stress. One may speculate that the mantle densities are related to the large-scale mantle dynamics that caused a crustal sag by a combination of lithospheric loading and drag at the base of the lithosphere due to downward-moving colder mantle. Hence, rifting processes are only of minor importance for the formation of the South and North eastern Barents Sea basins. An alternative model of crustal eclogitization (Hartz et al. 2007) has been mentioned, which gives a plausible explanation of the eastern Barents Sea basins, but requires a re-evaluation of seismic horizons and their geological meaning.

The PETROBAR Project has the ambition to link all the different approaches in a unified way to solve the relation between mantle and deep crustal structures and the basin formation in the Barents Sea. To understand the basin formation in the Eastern Barents Sea in more detail, one has also to look at the North, Central, and South Zemlya Basins, the flexural foreland basins of Novaya Zemlya, and try to understand their interaction with the East Barents Sea Basins.

Buiter & Torsvik (2007) studied the shortening associated with the displacement of Novaya Zemlya and the inversion of the East Barents Sea basins by combining numerical models and plate reconstructions. The East Barents Sea basins experienced mild inversion as the Siberian plate margin was pushed into Novaya Zemlya in the Late Triassic–Early Jurassic. Available (scarce) seismic interpretations indicate that the South and North East Barents Sea basins were only mildly deformed and that deformation was localised in the eastern part of the basin and at Novaya Zemlya. In the models, this is promoted by (1) a high strength of the lower crust, through either a high viscosity detachment or a strong creep law, (2) surface erosion and/or (3) small amounts of shortening. Novaya Zemlya may have been pushed westward in a thin-skinned manner. Part of the movement of the Siberian plate could be accommodated by

thrusts at Novaya Zemlya and perhaps in the domain of the Kara Sea at the western margin of the Siberian plate. Their models and plate reconstructions for the region indicate that the westward movement of Novaya Zemlya occurred in the Late Triassic–Early Jurassic (220–190 Ma) and was limited in magnitude to 100–200 km. These results provide valuable information for detailed models of the evolution of the East Barents Sea basins.

Interpretation of the elastic thickness distribution from inverse isostatic modelling to study the tectonic setting of the Barents Sea is a promising technique for the future as it allows a characterization of lithospheric structures over large areas as presented by Wienecke et al. (2007). However, the input data are crucial for such a study and an interpretation of the results presented in Wienecke et al. (2007) is as yet speculative. The critical point is the conversion of seismic velocities to densities, which is depending on the in situ pressure and temperature, as well as the rock composition. Further use of petrophysical measurements as done for the Western Barents Sea (Barrère et al. 2008) to constrain the conversions is needed, as well as an adjustment of modelled and observed gravity anomalies, to make a consistent interpretation. Therefore, further tests and re-calculations are needed.

An observation useful in characterising the tectonic setting of the Barents Sea is the apparent correlation between the presence of high-density material in the lower crust and the change in upper mantle densities. Comparison between basin geometry, distribution of high-density material and the magnetic anomalies points to the presence of intrusions along the transition zone, a feature often related to suture zones. However, the high-density distribution along the transition zone also coincides with a relatively thin lower crust (Ritzmann et al. 2007) and is the least constrained feature in our final model.

Despite this, the apparent correlation between the high-density feature in the lower crust and an aeromagnetic high along the transition zone points to the presence of intrusions at crustal levels above the lower crust. Here, further modelling is required to validate the interpretation, as our results are at present limited by the resolution of the Barents50 model (50x50 km resolution) and the distribution of deep seismic lines in the Barents Sea (only a few seismic transects that extend from the eastern to western Barents Sea are available). The precise location of these crustal structures must be the subject of more detailed studies in the future. Barrère et al. (2008) present such a detailed study for the western Barents Sea, which is linking the geological structures of mainland Finnmark to the western Barents Sea and towards Svalbard. Also in this

interpretation the Caledonian structures are not crossing into the eastern Barents Sea, but concentrate on the Norwegian part.

For the overall Barents Sea Region new regional models of the lithospheric structure will be made available within the PETROBAR Project. As a continuation of the ongoing project and the Barents3D compilation the new model will provide a basis for studying the lithospheric structure in more detail (e.g. Marelló et al. 2008). Detailed regional key transects which combine the basin configuration with the deep crustal and upper mantle structure will allow reconstructing the basin formation history of the East Barents Sea Basins. Hereby, inherited mantle structure is a key to unveil the post-rift evolution and subsidence history of the South and North eastern Barents Sea Basins in detail. Especially, changes in flexural rigidity with time due to thermal and tectonic events have to be considered to construct the present-day crustal configuration and potential field signal.

ACKNOWLEDGEMENTS

We appreciate the discussions with and the assistance from the following persons without whom the project would not have been possible: Bernhard Steinberger, Stephanie Werner, Trond Torsvik, Laurent Gernigon (all NGU), Oliver Ritzmann, Christian Weidle, Jan Inge Faleide, Nina Simon (all UiO), Tamara Litvinova (VSEGEI), Nils Maercklin (formerly NORSAR, now Naples), Federica Fratepietro, Ildiko' Nagy (both Trieste), and David Gee (Uppsala). Hans Morten Bjørnseth and Christine Fichler from StatoilHydro initiated our study and supplied us with information on the studied areas. We appreciate the assistance and help from all these persons and especially StatoilHydro for funding the study.

REFERENCES

- Åm, K. 1975: Aeromagnetic basement complex mapping north of latitude 62°N, Norway. *Norges geologiske undersøkelse* 316, 351-374.
- Arctic Gravity Project 2002: Arctic Gravity Project - Data Set Information. <http://earth-info.nga.mil/GandG/wgs84/agp/readme.html>
- Barrère, C., Ebbing, J. & Gernigon, L. 2008: Offshore prolongation of Caledonian structures and basement characterisation in the western Barents Sea from geophysical modeling. *Submitted to Tectonophysics Special Issue on "Progress in understanding sedimentary basins"*.
- Braitenberg, C., Ebbing, J. & Götze H.-J. 2002: Inverse modeling of elastic thickness by convolution method - The Eastern Alps as a case example. *Earth Planet. Sci. Lett.*, 202, 387-404.
- Braitenberg, C. & Ebbing, J. 2006: A study of large-scale basins and comparison to the Eastern Barents Sea basin. NGU Report 2006.081, 71pp.
- Braitenberg, C. & Ebbing, J. 2007: New insights into the West Siberian Basin from the satellite mission GRACE. NGU Report 2007.056, 64pp.
- Braitenberg C., Wienecke S. & Wang Y. 2006: Basement structures from satellite-derived gravity field: South China Sea ridge. *Journal of Geophysical Research*, 111, B05407, doi: 10.1029/2005JB003938
- Breivik, A., Mjelde, R., Grogan, P., Shimamura, H., Murai, Y. & Nishimura, Y. 2005: Caledonide development offshore–onshore Svalbard based on ocean bottom seismometer, conventional seismic, and potential field data. *Tectonophysics*, 401, 79–117.
- Buiter, S.J.H., Wortel, M.J.R., & Govers, R. 1998: The role of subduction in the evolution of the Apennines foreland basin, *Tectonophysics* 296, 249-268.
- Buiter, S. 2007: Unravelling the effective elastic thickness of the Barents Sea. NGU Report 2007.051, 33p.
- Buiter, S.J.H., & Torsvik, T.H. 2007: Horizontal movements in the eastern Barents Sea constrained by numerical models and plate reconstructions. *Geophys. J. Int.* (2007) 171, 1376–1389.
- Bungum, H., Ritzmann, O., Maercklin, N., Faleide, J., Mooney, W.D. & Detweiler, S.T. 2005: Three-Dimensional Model for the Crust and Upper Mantle in the Barents Sea Region. *EOS*, 86(16), doi: 10.1029/2005EO160003.
- Calmant, S. 1987: The elastic thickness of the lithosphere in the Pacific Ocean. *EPSL*, 85 277-288.

- Dziewonski, A.M. & Anderson, D.L. 1981: Preliminary reference earth model. *Phys. Earth. Plan. Int.*, 25, 297-356.
- Ebbing, J., Braitenberg, C. & Skilbrei, J.R. 2005: Basement characterisation by regional isostatic methods in the Barents Sea. NGU Report 2005.074, 78pp.
- Ebbing, J., Braitenberg, C. & Wienecke, S. 2007a: Insights into the lithospheric structure and the tectonic setting of the Barents Sea region from isostatic considerations. *Geophysical Journal International*, 171 (3), 1390–1403.
- Ebbing, J., Werner, S.C., Gernigon, L., Koren, T., Litvinova, T., Olesen, O., Saintot, A., Smelror, M., Petrov, O. and Sobolev, N. 2007b: Transition from rift basins to intra-cratonic basins in the Barents Sea as revealed in potential field signature and paleogeography. *Eos Trans. AGU*, 88(52), *Fall Meet. Suppl.*, Abstract T13D-1568.
- Faleide, J.I., Myhre, A.M. and Eldholm, O. 1988: Early Tertiary Volcanism at the western Barents Sea margin. In: A.C. Morton and L.M. Parson (Editors), *Tertiary Volcanism and the Opening of the NE Atlantic.*, Geological Society Special Publication, pp. 135-146.
- Faleide, J.I., Gudlaugsson, S.T., Eldholm, O., Myhre, A.M. and Jackson, H.R. 1991: Deep Seismic Transects across the Sheared Western Barents Sea-Svalbard Continental-Margin. *Tectonophysics* 189(1-4): 73-89.
- Faleide, J.I., Vågnes, E. & Gudlaugsson, S.T. 1993: Late Mesozoic-Cenozoic evolution of the southwestern Barents Sea in a regional rift-shear tectonic setting. *Marine Petrol. Geol.* 10, 186-214.
- Faleide, J.I., Solheim, A., Fiedler, A., Hjelstuen, B.O., Andersen, E.S. & Vanneste, K. 1996: Late Cenozoic evolution of the western Barents Sea-Svalbard continental margin. *Global and Planetary Change* 12, 53-74.
- Faleide, J.I., Ritzmann, O., C. Weidle, C. & A. Levshin, A. 2006: Geodynamical aspects of a new 3D geophysical model of the greater Barents Sea region – Linking sedimentary basins to the upper mantle structure. *Geophysical Research Abstracts*, 8, 08640.
- Fichler, C., Rundhovde, E., Johansen, S. & Sæther, B.M. 1997: Barents Sea tectonic structures visualized by ERS1 satellite gravity data with indications of an offshore Baikalian trend. *First Break*, 15.11, 355-363.
- Förste, C., Schmidt, R., Stubenvoll, R., Flechtner, F., Meyer, U., König, R., Neumayer, H., Biancale, R., Lemoine, J.-M., Bruinsma, S., Loyer, S., Barthelmes, F., & Esselborn, S. 2007: The GeoForschungsZentrum Potsdam/Groupe de Recherche de Geodesie Spatiale satellite-only and combined gravity field models: EIGEN-GL04S1 and EIGEN-GL04C. *Journal of Geodesy*, doi:10.1007/s00190-007-0183-8.

- Gabrielsen, R.H., Færseth, R.B., Jensen, L.N., Kalheim, J.E. & Riis, F. 1990: Structural elements of the Norwegian continental shelf. Part I: The Barents Sea Region. *Norwegian Petroleum Directorate Bulletin* 6, 33pp.
- Gee, D. G. 2004: The Barentsian Caledonides: Death of the High Arctic Barents Craton. In: Smelror M. and Bugge T. (eds.) *Arctic Geology, Hydrocarbon Resources and Environmental challenges*. Abstracts and Proceedings of the Geological Society of Norway 2, 48-49.
- Gee, D.G. & Pearce, V. 2006: The Neoproterozoic Timanide Orogen of eastern Baltica: Introduction. In: Gee, D.G. & Pearce, V. (eds.) *The Neoproterozoic Timanide Orogen of eastern Baltica. Geological Society of London Memoirs* 30, 1-3.
- Gramberg, I.S., Glebovsky, V. Y., Grikuro, G.E., Ivanov, V.L., Korago, E.A., Kos'ko, M.K., Maschenkov, S.P., Piskarev, A.L., Pogrebitsky, Y.E., Shipelkevitch; Y. V. & Suprunenko, O.I. 2001: Eurasian Arctic Margin: Earth Science Problems and Research Challenges. *Polarforschung* 69, 3-15.
- Gudlaugsson, S.T., Faleide, J.I., Johansen, S.E. & Breivik, A.J. 1998: Late Palaeozoic structural development of the south-western Barents Sea. *Marine and Petroleum Geology* 15, 73-102.
- Hartz, E. H., Podladchikov, Y. Y., Medvedev, S., Faleide, J.I. & Simon, N. S. C. 2007: Force, energy and mass balanced basin models: New concepts and Arctic examples. *Geophysical Research Abstracts* 9, 10468.
- Ivanova, N.M., Sakoulina, T.S. & Roslov, Yu.V. 2006: Deep seismic investigation across the Barents–Kara region and Novozemelskiy Fold Belt (Arctic Shelf). *Tectonophysics* 420, 123–140.
- Johansen, S.E., Ostisty, B.K., Birkeland, Ø., Fedorovsky, Y.F., Martirosjan, V.N., Christensen, O. B., Cheredeev, S.I., Ignatenko, E.A. & Margulis, L.S. 1992: Hydrocarbon potential in the Barents Sea region: play distribution and potential. In: *Arctic Geology and Petroleum Potential*. In: Vorren, T.O., Bergsager, E., Dahl-Stammes, Ø.A., Holter, E., Johansen, B., Lie, E. and Lund, T.B. (eds.) *NPF Special Publication* 2, 273-320.
- Kaus, B.J.P., Connolly, J.A.D., Podladchikov, Y.Y. & Schmalholz, S.M. 2005: The effect of phase transitions on sedimentary basin subsidence. *Earth and Planetary Science Letters* 23, 213-228.

- Levshin, A.L., Schweitzer, J., Weidle, C., Shapiro, N.M. & Ritzwoller, M.H. 2007: Surface wave tomography of the Barents Sea and surrounding regions. *Geophys. J. Int.* 170, 441–459.
- Lowry, A.R. & Smith, R.B. 1994: Flexural rigidity of the Basin and Range–Colorado Plateau–Rocky Mountain transition from coherence analysis of gravity and topography. *J. Geophys. Res.* 99, 20123–20140.
- McKenzie, D. 1978: Some remarks on the development of sedimentary basins. *Earth and Planetary Science Letters* 40, 25–32.
- Nunn, J.A. 1994: Free thermal convection beneath intracratonic basins: thermal and subsidence effects. *Basin Research* 6, 115–130.
- O'Leary, N., White, N., Tull, S. & Bashilov, V. 2004: Evolution of the Timan–Pechora and South Barents Sea basins. *Geol. Mag.* 141 (2), 141–160.
- Olesen, O., Roberts, D., Henkel, H., Lile, B.L. & Torsvik, T.H. 1990: Aeromagnetic and gravimetric interpretation of regional structural features in the Caledonides of West Finnmark and North Troms, northern Norway. *Norsk Geologisk Tidsskrift* 419, 1–24.
- Popowski, T., Connard, G. & French, R. 2006: *GMSYS-3D: 3D Gravity and Magnetic Modeling for OasisMontaj - User Guide*. Northwest Geophysical Associates, Corvallis, Oregon.
- Ritzmann, O., Maercklin, N., Faleide, J.I., Bungum, Mooney, W.D. & Detweiler, S.T. 2007: A three-dimensional geophysical model of the crust in the Barents Sea region: model construction and basement characterization. *Geophys. J. Int.* 170, 417–435.
- Roy, M., MacCarthy, J.K. & Selverstone, J. 2005: Upper mantle structure beneath the eastern Colorado Plateau and Rio Grande rift revealed by Bouguer gravity, seismic velocities and xenolith data. *G³: Geochemistry Geophysics Geosystems* 6(10), doi:10.1029/2005GC001008.
- Skilbrei, J.R. 1991: Interpretation of depth to the magnetic basement in the northern Barents Sea (south of Svalbard). *Tectonophysics* 200, 127–141.
- Skilbrei, J.R. 1995: Aspects of the geology of the southwestern Barents Sea from aeromagnetic data. *NGU Bulletin* 427, 64–67.
- Skilbrei, J.R., Habrekke, H., Christoffersen, T. & Myklebust, R.A. 1990: Aeromagnetic surveying at high latitudes, a case history from the Northern Barents Sea. *First Break* 8, 46–50.
- Skilbrei, J.R., Skyseth, T. & Olesen, O. 1991: Petrophysical data and opaque mineralogy of high-grade and retrogressed lithologies - Implications for the interpretation of

- aeromagnetic anomalies in Northern Vestranden, Central Norway. *Tectonophysics* 192, 21-31.
- Sloss, L.L., and Scherer, W. 1975: Geometry of sedimentary basins: applications to the Devonian of North America and Europe. *Geol. Soc. Am. Memoir* 142, 71-88.
- Stewart, J. & Watts, A.B. 1997: Gravity anomalies and spatial variations of flexural rigidity at mountain ranges. *J. Geophys. Res.* 102, 5327-5253.
- Tsikalas, F., 1992: *A study of seismic velocity, density and porosity in Barents Sea wells (N. Norway)*. Master Thesis, Department of Geology, University of Oslo, Norway.
- Turcotte, D.L. & Schubert, G. 1982: *Geodynamics: Applications of continuum physics to geological problems*. John Wiley and Sons, New York.
- Vening Meinesz, F.A. 1939: Tables fondamentales pour la réduction isostatique régionale. *Bulletin Géodésique* 63, 711 – 776.
- Werner, S.C., Ebbing, J., Kihle, O., Litvinova, T. and Olesen, O., 2007: Potential field data of the Barents- and Kara Seas – Reevaluated. Arctic Conference Days, Tromsø.
- Wienecke, S. 2006: *A new analytical solution for the calculation of flexural rigidity: Significance and applications*. PhD thesis, Freie Universität Berlin.
- Wienecke, S., Ebbing, J. & Gernigon, L. 2007: 3D density modelling, isostasy and elastic thickness calculation of the Barents Sea. NGU Report 2007.022. 56pp.

LITS OF FIGURES

Figure 2.1 Overview map of the Barents Sea and surrounding regions (redrawn from Ritzmann et al. 2007). BB: Bjørnøya Basin; BF: Billefjorden Fault; FP: Finnmark Platform; FJL: Franz-Josef Land; GH: Gardabanken High; HB: Hammerfest Basin; KP: Kola Peninsula; KR: Knipovich Ridge; LH: Loppa High; MR: Mohns Ridge; MS: Mezen Syncline; NB: Nordkapp Basin; OB: Olga Basin; SB: Sørvestnaget Basin; SBH: Sentralbanken High; SH: Stappen High; SKB: Sørkapp Basin; SKZ: Sørkapp Fault Zone; SJZ: Senja Fracture Zone; TB: Tromsø Basin; VVP: Vestbakken Volcanic Province; YP: Yermak Plateau. Top insert shows a geological profile from the Knipovich Ridge to the Kara Sea (A-A').

Figure 2.2 a) Depth to basement and b) depth to Moho maps. The maps are adopted from the Barents50 model (Ritzmann et al. 2007) with modifications after Skilbrei (1991, 1995) for the western Barents Sea. The black dotted lines denote the location of the regional seismic lines used in compiling the Barents 50 model.

Figure 2.3 Presentation of the spatial resolution of the Barents50 and the utilized seismic profiles (in colour) (Ritzmann et al. 2007).

Figure 2.4 Bouguer anomaly map of the Barents Sea as compiled by the NGU-VSEGEI cooperation project (Werner et al. 2007).

Figure 2.5 Magnetic anomaly map of the Barents Sea as compiled by the NGU-VSEGEI cooperation project (Ebbing et al. 2007b).

Figure 3.1 Map showing the gravity effect of the simple 3D density model based on constant densities for the crust and mantle, a density-depth relation for sedimentary rocks and geometry from Fig. 2.1. b) The residual field shows large regional differences between the gravity effect of the 3D model and the observed Bouguer gravity. The profile marked A – A' is plotted in Fig. 3.2.

Figure 3.2 West-east profile through the model from the westernmost border of the Barents Sea to the Kara Sea showing the geometry and density distribution of the initial 3D density model. The upper panel shows the large differences between the modelled gravity effect (green line) and the observed Bouguer anomaly (red line). Profile location in Fig. 3.1.

Figure 3.3 The simple Airy isostatic Moho depth (root) was calculated by taking into account the loading of bathymetry/topography and sedimentary rocks as well as a density contrast between the lower crust and upper mantle of 400 kg/m^3 and a relative normal crustal thickness of 35 km.

Figure 3.4 Maps showing (a) lower crustal density and (b) lithospheric mantle density variations. The varying densities allow local isostatic equilibrium to be achieved and give a modelled gravity field that fits the observed gravity to a large degree. The profile marked A – A' is plotted in Fig. 3.5.

Figure 3.5 Profiles showing the same geometry as in Fig. 3.2, but in (a) the densities of the lithospheric mantle are varied to isostatically balance the lithosphere, and in (b) densities in the lower crust are also varied to reduce the misfit for intermediate- and short-wavelength gravity anomalies whilst maintaining isostatic balance. The gravity residuals of the entire 3D model are shown in Figs. 3.6 (a) and (b).

Figure 3.6 Maps showing residual gravity for the 3D models. (a) Gravity residual for the model that includes only isostatic mantle densities and the intra-crustal horizon in the computation. (b) Gravity residual for the model that also includes small lower-crustal density variations. Profile A – A' is plotted in Figs. 3.5 (a) and (b).

Figure 3.7 Example of the BARMOD velocity model along a west-east section at latitude 73° N. Shown are the S-wave velocities. Profile location in Fig. 3.8.

Figure 3.8 (Left) Depth slice through the BARMOD tomography model and (right) lithospheric mantle velocity perturbation (Faleide et al. 2006).

Figure 3.9 Geoid model defined from spherical harmonics to degree 360, corresponding to a wavelength resolution of >111 km (data from Förste et al. 2007).

Figure 3.10 Geoid undulation defined in a wavelength range from 111 km to 2666 km.

Figure 3.11 Geoid undulation defined in a wavelength range from 111 km to 2000 km.

Figure 3.12 Geoid undulation and gravity effect of the high-velocity/high-density body in the upper mantle (density contrast of +10 kg/m³ to surrounding).

Figure 4.1 Outline of basins in the Barents Sea (after Ritzmann et al. 2007) on top of the isostatic lower crustal density distribution as presented in Fig. 3.4a

Figure 4.2 Contours of the lower crustal density distribution (Fig. 3.4a) on top of the magnetic anomaly map of the Barents Sea (Fig. 2.5). The bold grey polygon line indicates the outline of the North and South eastern Barents Sea mega-basins.

Figure 4.3 Magnetic anomaly (left) and interpretation of different magnetic domains (right), reflecting different geological provinces. Blue lines = magnetic trends. Magnetic domains: D1 - Precambrian Shield; D2- Oceanic Crust; D3- Cretaceous Volcanic Area; D4- East-West Barents Sea Transition zone; D5- Western Barents Sea basement (from Barrère et al. 2008).

Figure 5.1 On the left side: elastic thickness distribution calculated with the ASEP and constant Young's modulus of 100 GPa. On the right side: elastic thickness distribution calculated with the ASEP and Young's modulus variation shows high elastic thickness values variation in the middle part of study area (40 longitude) (from Wienecke et al. 2007).

Figure 5.2 Thickness of the crust and sedimentary cover along Profile 1 (see Fig. 2.1 for location), after Ritzmann et al. (2007) and (above) the vertical load exerted by the water and sedimentary layers.

Figure 5.3 Airy isostatic deflection compared to basement depth along Profile 1. Density of mantle is 3300 kg m^{-3} , the density of the sedimentary rocks is depth-dependent (an average of 2600 kg/m^3 is adopted) (Buitter 2007).

Figure 5.4 Flexure of a thin elastic plate along Profile 1. a) Deflection of plates with elastic thickness 10 and 30 km compared to basement depth. The elastic plate is loaded by water and sediments b) Deflection of an elastic plate with thickness 10 km compared to the Moho. The plate is loaded by water, sediments and crustal density differences (Buitter 2007).

Figure 5.5 (top) The forward model applied in Buitter (2007) uses the full load of the water and sedimentary layers to calculate the basement deflection. If the deflection of the crust-mantle interface is calculated, the loads caused by lateral density and thickness changes in the crust are also taken into account. The crustal reference column then uses the average crustal thickness along the profile (e.g., $h_c = 24.9 \text{ km}$ along profile 1). (below) The ASEP method used by Wienecke et al. (2007) refers all densities, including those of the water and sediment layers, to a reference column. In the Barents Sea area, Wienecke et al. (2007) use a crustal thickness of 30 km. However, the crust-mantle interface in the Barents Sea area is on average deeper than 30 km in the Barents Sea area



Norges geologiske undersøkelse
Postboks 6315, Sluppen
7491 Trondheim, Norge

Besøksadresse
Leiv Eirikssons vei 39, 7040 Trondheim

Telefon 73 90 40 00
Telefax 73 92 16 20
E-post ngu@ngu.no
Nettside www.ngu.no

*Geological Survey of Norway
PO Box 6315, Sluppen
7491 Trondheim, Norway*

*Visitor address
Leiv Eirikssons vei 39, 7040 Trondheim*

*Tel (+ 47) 73 90 40 00
Fax (+ 47) 73 92 16 20
E-mail ngu@ngu.no
Web www.ngu.no/en-gb/*